2003

EVALUATION OF FLOW DYNAMICS THROUGH AN ADJUSTABLE SYSTEMIC-PULMONARY ARTERY SHUNT

Timothy Brown
University of Kentucky, timothybrown_uk@yahoo.com

ABSTRACT OF THESIS

EVALUATION OF FLOW DYNAMICS THROUGH AN ADJUSTABLE SYSTEMIC-PULMONARY ARTERY SHUNT

An adjustable systemic-pulmonary artery (SPA) shunt is being developed that consists of a polytetrafluoroethylene (PTFE) graft with a screw plunger mechanism. This device would allow full control of flow through SPA shunts used to augment pulmonary blood flow in neonates born with single ventricle physiology. The objective of this study is to evaluate the changes this mechanism has on flow fields for a 4 mm and 5 mm adjustable SPA shunt. Two *in vitro* models were examined; an idealized model with an axisymmetric constriction and a model developed from 3-D reconstruction of the actual shunt under asymmetric constriction. These models were used to measure the instantaneous velocity and vorticity fields using Particle Image Velocimetry (PIV) under both steady and pulsatile flow conditions. Recirculation regions and maximum values of velocity, vorticity, and shear stress are compared between the 4 mm and 5 mm models. The results indicate that for the idealized model of both shunts, separation regions are much smaller, persisting for approximately 0-1.75 diameters downstream of the constriction, while for the realistic models separation regions of 2.5 diameters downstream were observed. Additional models of a 4 mm and 5 mm shunt were tested under pulsatile conditions matching R_e of 1061 and 849 and a Womersley number of 4.09 and 5.12, respectively, as seen *in vivo*. The maximum shear rates observed in both shunts are within an allowable range without inducing platelet aggregation or hemolysis. However, regions of reverse flow exist distal to the throat, leading to possible concerns of plaque formation. Further *in vivo* testing will be needed to address this concern. This work is part of an extensive effort in developing a completely implantable adjustable systemic-pulmonary artery shunt.

Keywords: systemic-pulmonary artery, SPA, shunt, adjustable, PIV, particle image velocimetry, flow separation, shear rate, vorticity, flow rate, steady, pulsatile

Timothy Brown

08/01/03

EVALUATION OF FLOW DYNAMICS THROUGH AN ADJUSTABLE SYSTEMIC-PULMONARY ARTERY SHUNT

By

Timothy Brown

Dr. Charles Knapp
(Director of Thesis)

Dr. David Puleo
(Director of Graduate Studies)

08/01/03
(Date)

RULES FOR THE USE OF THESES

Unpublished Theses submitted for the Master's degree and deposited in the University of Kentucky Library are as a rule open for inspection, but are to be used only with due regard to the rights of the authors. Bibliographical references may be noted, but quotations or summaries of parts may be published only with the permission of the author, and with the usual scholarly acknowledgments.

Extensive copying or publication of the thesis in whole or in part requires also the consent of the Dean of The Graduate School of the University of Kentucky.

THESIS

Timothy Brown

The Graduate School
University of Kentucky
2003

EVALUATION OF FLOW DYNAMICS THROUGH AN ADJUSTABLE SYSTEMIC-PULMONARY ARTERY SHUNT

THESIS

A thesis submitted in partial fulfillment of the
requirements for the degree of Master of Science
in the College of Engineering
at the University of Kentucky

By

Timothy Brown

Lexington, Kentucky

Director: Dr. Charles Knapp, Department of Biomedical Engineering

Co-Director: Dr. Jamey Jacob, Department of Mechanical Engineering

Lexington, Kentucky

2003

Acknowledgments

Timothy would like to acknowledge the department of Cardiothorasic Surgery at the University of Kentucky Chandler Medical Center and the Kentucky Science and Engineering Foundation (KSEF) for funding for the project. He would also like to thank his two advisors, Dr. Charles Knapp and Dr. Jamey Jacob, for their unending supply of knowledge and wisdom in helping overcome the many obstacles reached during the study.

Table of Contents

List of Tables

List of Figures

List of Files

TMBrown_Thesis.pdf	6.94 MB PDF file.

Chapter 1

Introduction

Systemic-pulmonary artery (SPA) shunts are connections used to improve pulmonary blood flow in patients suffering from a type of congenital heart disease known as single ventricle physiology (SVP). The SPA shunt is a simple synthetic vascular graft made from either polytetrafluroethylene (PTFE) or Dacron that ranges in size from 3.0 mm to 4.0 mm in diameter. One end of the shunt is connected to the innominate or subclavian artery, and the other end to the pulmonary artery [1]. During the first three months of development, the lower part of a fetal heart normally divides into two pumping chambers: the left ventricle and the right ventricle. However, there are rare cases in which this normal separation does not occur. As a result, the infant is born with a single ventricle. Oxygen-rich blood and oxygen-poor blood then mix together instead of remaining separate in the two ventricles. Only some of the oxygen-rich blood travels to the rest of the body. Newborns undergo placement of an SPA shunt to increase blood flow to the lungs, thus providing more oxygen-rich blood to the body. The ratio of pulmonary:systemic blood flow (Qp:Qs), which ideally is 1:1, is crucial for the survival of the infant in the hours following major cardiac surgery, yet it is very difficult to control the blood flow with existing SPA shunts [2].

The Center for Biomedical Engineering and the Chandler Medical Center at the University of Kentucky are currently developing an adjustable SPA shunt that would allow full control of blood flow between the systemic and pulmonary circulation at all times after implantation. However, a major concern with an adjustable SPA shunt is the possibility of mechanical damage to blood cells due to the changes in the flow field. Blood flow in a stenotic vessel such as a constricted shunt follows a complex pattern of flow dynamics. Flow rate increases considerably in the stenosis before surging downstream to post-stenosis low flow, where regions of recirculation can exist depending upon the severity of the constriction [3]. This type of complex flow pattern, shown in Figure 1.1, results in high shear stress through the throat of the stenosis and very low shear stress in the region

immediately after the constriction. Particle velocities, areas of flow reversal, and vorticity all have an impact in the clinical setting as increased velocity and shear stress can lead to rupture of red blood cells (hemolysis) and induce platelet aggregation [4]. Areas of low flow or recirculation have been shown to promote cell-cell collision, which could also promote platelet adhesion [3].

1.1 Objective

The objective of this work was to evaluate the changes in flow fields through an adjustable systemic-pulmonary artery shunt using an *in vitro* circulatory model with a fluid that simulates blood. Results from this study can be used to predict the *in vivo* effects of an adjustable SPA shunt on blood cells.

1.2 Outline of Thesis

The experiments contained within this thesis are part of a multi-faceted approach towards developing a completely implantable adjustable SPA shunt. By creating actual models of various constrictions of an adjustable shunt, flow fields can be analyzed without immediately resorting to costly and time consuming animal studies. The focus of this work is divided into two main steps: (1) the development of optically clear flow models of asymmetrically and axisymmetrically constricted SPA shunts, and (2) evaluation of flow dynamics through *in vitro* testing of these flow models using particle image velocimetry (PIV).

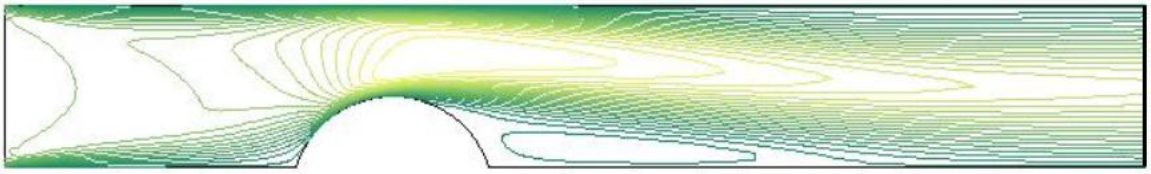

Figure 1.1: Illustration of complex flow pattern through a stenotic vessel. Typically, shear stress is very high at the throat and very low in regions of recirculation immediately after the stenosis.

Chapter 2

Background

2.1 The Need for an Adjustable SPA Shunt

Probably the most common type of SVP and certainly the most important need for an adjustable SPA shunt is hypoplastic left heart syndrome (HLHS) [5]. HLHS is seen in approximately 700 to 1000 births/year in the United States, and despite improvements in diagnosis, medical management and surgical procedures, HLHS remains the leading cause of cardiac death among newborns [2]. In this lethal case of SVP, the entire left side of the heart becomes underdeveloped and is unable to support the necessary circulation (Figure 2.1). The infant must then depend solely on the right ventricle to sustain life [6].

There are basically two options for a child born with HLHS: Cardiac transplantation or a 3-stage surgical procedure. The percentage of patients choosing cardiac transplantation is declining due to a limited number of donors and the constant risk of rejection [7]. The first of three operations for the surgical option is the Norwood procedure, which is performed during the first two weeks of life. The Norwood operation involves reconstruction of the aorta and pulmonary arteries so that the flow of blood from the right ventricle is directed primarily to the remodeled and augmented aorta. Blood flow to the lungs is then supplied by an SPA shunt (Figure 2.2).

Even in very current series from established centers, mortality for the Norwood procedure is 15%-25% or higher [8]. It is crucial for survival that there be an appropriate balance between the systemic and pulmonary circulations. The Norwood circulation is optimized when pulmonary and systemic perfusions are equal. Too little pulmonary blood flow leads to hypoxia and death, while too much pulmonary blood flow leads to systemic underperfusion, with subsequent acidosis and death. A study determining the causes of death after the Norwood procedure found that of the 122 postmortem cases, 19% died because of excessive pulmonary blood flow, while 17% died due

to obstruction of pulmonary arterial blood flow [9]. Currently, Qp:Qs is maintained by carefully choosing the best size shunt for the patient at the time of surgery, which cannot be further modified. Any further balance is accomplished by medical (i.e., non-surgical) means, including adjusting the oxygen level on the ventilator, administering vasodilators, etc. However, these maneuvers are imprecise, have limits in their extent of action, and have unwanted hemodynamic side effects [10]. If a patient survives the Norwood procedure, the SPA shunt is removed at approximately 6 months of age when the second stage of operations, which is known as the Hemi-Fontan operation, is performed. An adjustable SPA shunt will thus provide the necessary balance between systemic and pulmonary flow, hopefully leading to a decrease in mortality rates among infants.

2.2 Previous Work

The following sections summarize previous work on manipulating shunt flow in infants following a first-stage Norwood operation. These techniques described below do not include current methods of administrating vasodilators or vasoconstrictors.

2.2.1 Placement of an Adjustable Tourniquet around an SPA Shunt

Schmid *et al.* [11] reported the clinical results of an adjustable tourniquet placed around an SPA shunt used in 7 of the 26 infants who underwent first-stage palliative Norwood operation between 1995 and 1998. The banding, or tourniquet, was produced using a 7-0 Prolene suture passed through an 8F polyethylene tube. The banding was tightened until the desired shunt diameter was reached and then hemostatic clips were applied on the Prolene suture to hold it in position. Adjustments to the banding were made to achieve an arterial saturation of 75% to 85%. The total mortality reported was 27% (7 of 26 patients), although all 7 patients who received the adjustable tourniquet around the shunt survived. There was no significant difference in the preoperative hemodynamic profile between patients who received and those who did not receive constricting of the shunt. The tourniquet was further adjusted when systemic arterial oxygen saturation was in excess of 85%, which occurred in two patients who had the tourniquet adjusted more than once in the postoperative period. In 5 patients, the tourniquet was removed during delayed sternal closure, while it was left in place in the remaining 2 patients and removed during the hemi-Fontan operation without any problems. Schmid noted that the banding of the shunt by a 7-0 Prolene can be reopened by balloon angioplasty if necessary, although this was not needed in any of the reported cases. No problems with the constricted shunt were seen postoperatively after hospital discharge of the patients. The advantage to this technique is that snaring of the shunt results in an

immediate change in pulmonary blood flow. However, it is difficult to control the percent reduction in shunt flow due to the constriction, and once the desired flow rate is finally achieved and the chest closed, the shunt can no longer be modified.

2.2.2 Dilatable Banding of an SPA Shunt

Chikada *et al.* [12] describe the case of a neonate with excessive pulmonary blood flow following a first-stage Norwood operation. A 3.5 mm PTFE graft was used in the procedure, in which immediate postoperative complications arose due to high pulmonary blood flow. The brachiocephalic artery, proximal to the anastomosis of the shunt, was banded with a PTFE graft to lower systemic oxygen saturation (90%). The banding was fixed with a 5-0 absorbable polydioxanone suture. Metabolic acidosis improved after banding and arterial oxygen saturation decreased to 80%. At 3 months of age the patient had to undergo balloon angioplasty because of low systemic oxygen saturation. The polydioxanone suture was easily cut by the balloon dilatation and the banding was loosened. No further complications were seen and the left ventricle volume of the patient increased gradually. The problems, however, with this technique are that (1) it is difficult to control the reduction in shunt flow with the banding and (2) balloon angioplasty is needed if the patient outgrows the restricted pulmonary blood flow. Other methods have also been reported of pulmonary artery banding using different absorbable sutures.

2.2.3 Use of a Hemostatic Clip for Adjusting an SPA Shunt

Kuduvalli *et al.* [13] describe a method for restricting flow through an SPA shunt by application of a hemostatic clip. The technique was used in 6 patients who underwent a first-stage Norwood operation receiving a 3.5 mm expanded PTFE shunt. The goal post-operatively was to maintain systemic oxygen saturation of around 75%-85%. The shunts were downsized from 3.5 mm to 3.0 mm by clamping with a medium-sized Ligaclip. Till publication, no thrombogenic complications from clipping the shunts had been observed. However, all of the patients received heparin intravenously in the early postoperative period until they were converted to enteric aspirin. Angiography performed on one child preceding the hemi-Fontan procedure showed clear patency of the clipped shunt. The benefits of this technique are that it is quick and very simple. Surgical revision of the shunt is avoided, and removal of the clip, if necessary, is fairly easily accomplished. The disadvantage, though, is the lack of accuracy in reducing the size of the shunt. Slipping of the clip off the shunt was also noted as a possible problem. Moreover, shunt flow cannot be adjusted once delayed sternal closure has been completed.

Additional studies involving 3-D simulation of an SPA shunt using computational fluid dynamics [14] have been conducted, as well as those using mathematical models of the Norwood circulation to examine the effects of shunt size, vascular resistance, and heart rate [15]. However, none of these studies involve the investigation of flow dynamics through a constricted SPA shunt, namely because no device currently exists.

2.3 Prototype Development of an Adjustable SPA Shunt

Although the development of the actual device and the controller unit that will allow precise control of shunt flow postoperatively are beyond the scope of this thesis, a brief overview of the prototype used in the study is presented below. The main goals in the design of the device are as follows:

1. Number of potential settings: The minimum number of different settings to control shunt flow should range from 8-10. This should be sufficient to keep the Qp:Qs in an optimal range for any patient.

2. Discreet settings: It is important that the shunt resistance be in discreet settings. This will allow a clinician to return to the original setting easily if a given change does not result in favorable improvement.

3. Frequency of Adjustments: A child's physiological state may change rapidly in the early postoperative period after a Norwood procedure. Therefore, the design must allow for unlimited number of adjustments as often as every few minutes. Adjustments must be possible until removal of the device in case the infant outgrows the current setting.

4. No internal power source: The implantable device will not require an internal power source. This would eliminate the concern over battery life or the need for electrical connections traversing the skin.

5. Biocompatibility: The device must be compatible with blood, minimizing concerns of thrombosis and hemolysis.

The initial design involved the use of a bladder that produced an ideal axisymmetric constriction around the shunt. This type of constriction would be optimal for reducing shear stresses and maximum velocities through the throat of the shunt. However, due to problems with wrinkling of the shunt and other design challenges, a mechanism constricting only one side of the wall was used

instead to adjust the resistance of the SPA shunt, a design resulting in an asymmetric constriction. The prototype can be broken down into the following key subcomponents: a variable resistance mechanism, a torque producing unit (TPU), and a controller unit (CU).

2.3.1 Variable Resistance Mechanism

A schematic of the device that has been constructed is shown in Figure 2.3. The prototype utilizes a screw-plunger mechanism to control resistance within the graft. A silastic sleeve maintains a bolt in a fixed position relative to the center of the graft. A metal cable with screw threads (corresponding to the bolt) terminates in a plunger, which sits next to the graft (Figure 2.4). Rotation of the cable causes linear displacement of the plunger, via the screw mechanism, relative to the center of the graft. The plunger can be used to increase or decrease the effective diameter of the graft, and therefore its resistance. The prototype as pictured has a hand knob to turn the cable/screw/plunger mechanism.

2.3.2 Torque Producing Unit

The TPU, which is used to turn the cable inside the body, would replace the hand knob used in this study. It would remain fastened by sutures to the underneath side of the right anterior chest wall of the infant. The TPU consists of a magnetic disk, which is coupled to the cable driving the plunger mechanism. The magnetic disk has grooves along the circumference on its underneath side. The housing has corresponding grooves that interlock with the grooves on the magnetic disk. A spring mechanism keeps the magnetic disk firmly adjacent to the housing, thus preventing the disk from rotating. To adjust the diameter of the shunt, an external magnet is placed over the TPU (in the clinical situation, the external magnet is placed over the right anterior chest wall). This is shown in Figure 2.5. The external magnet pulls the magnetic disk in the TPU against the spring and away from the interlocking mechanism of the housing. Rotating the external magnet can now be performed to rotate the disk and thus the cable. This is translated by the screw plunger mechanism into a linear displacement of the plunger decreasing (or increasing) the diameter, and therefore the resistance of the graft.

2.3.3 Controller Unit

The CU is the only component that remains outside of the patient. Thus, it has none of the compatibility/miniaturization issues in common with the other components. Power issues are minimal, as it would be very feasible to utilize a unit that had a wall plug-in power source. The

current idea for a CU is an electromagnet. The final goal of the CU will include a mechanism that is able to provide discreet rotation (corresponding to appropriate rotation of the magnetic disk in the TPU).

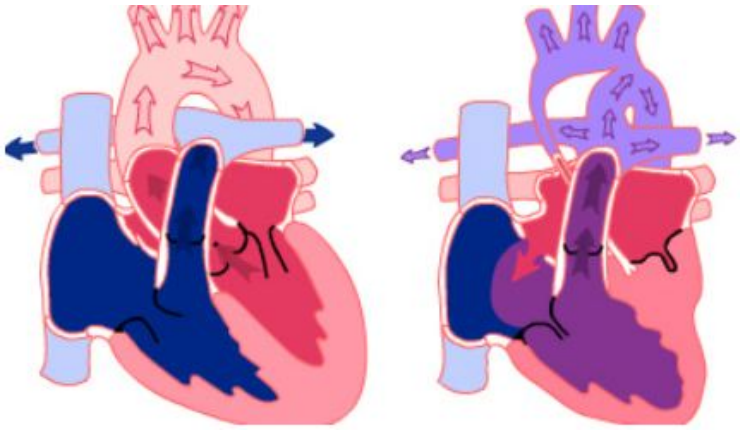

Figure 2.1: Normal heart (left) and Hypoplastic Left Heart Syndrome (right); HLHS is terminal within days after birth [16]. Blue and red regions indicate oxygen-poor and oxygen-rich blood, respectively, while violet regions indicate the mixture of both oxygen-rich and oxygen-poor blood.

Figure 2.2: Norwood procedure used to correct Hypoplastic Left Heart Syndrome by implanting a systemic-pulmonary artery shunt [16].

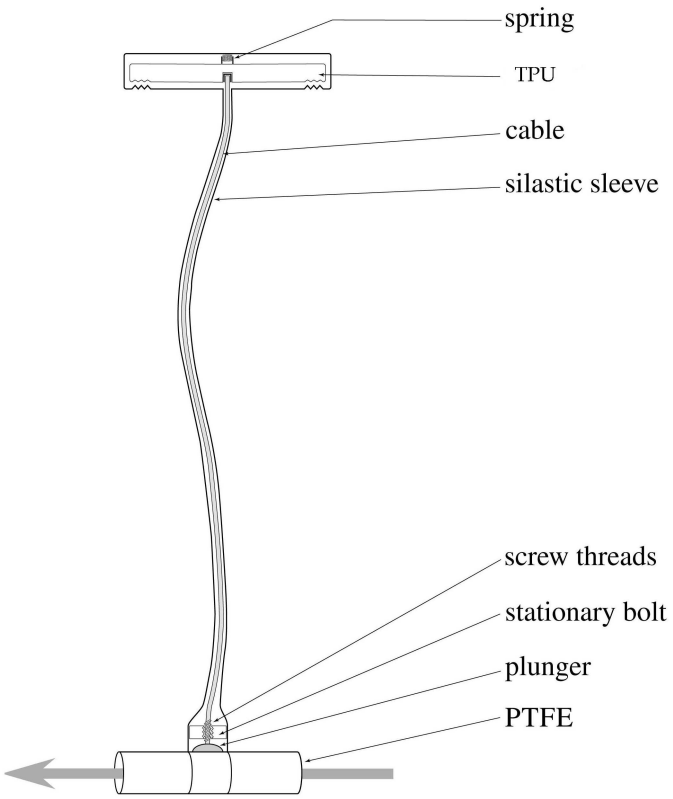

Figure 2.3: Schematic of the prototype of an adjustable SPA shunt. This device is fully implantable in the infant's body.

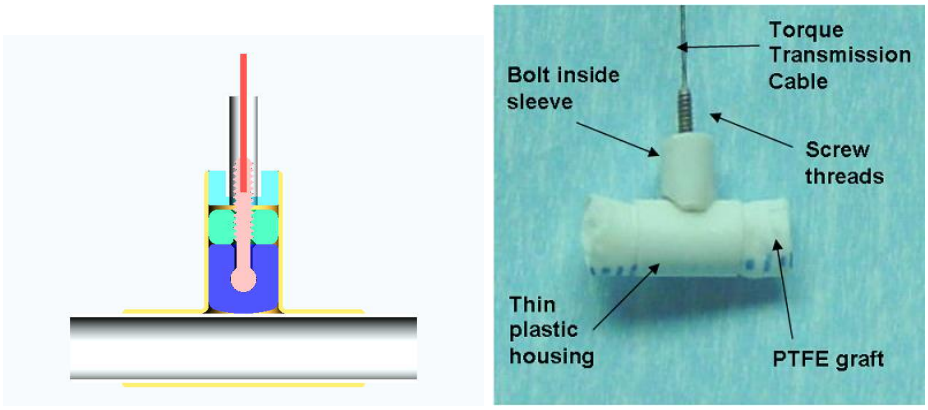

(a) (b)

Figure 2.4: Detailed view of the constriction mechanism. The image on the left shows a CAD model of the future constriction mechanism. The actual prototype used in this study is shown on the right.

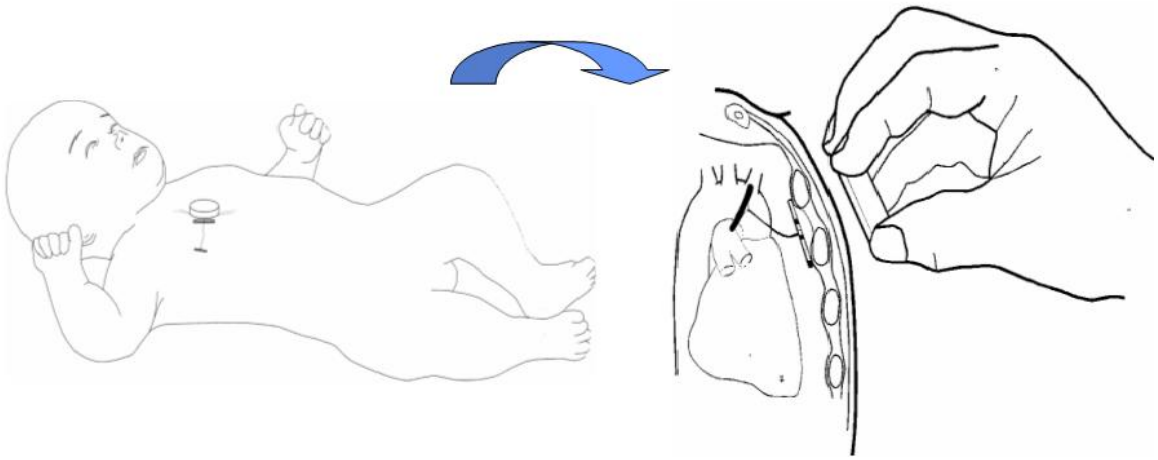

Figure 2.5: The controller unit (CU) will be placed on the right anterior chest wall to change the setting on the adjustable SPA shunt.

Chapter 3

Theory

This chapter provides a brief overview of the fluid mechanics related to this study. The following sections discuss the equations governing steady and pulsatile flow, as well as the conditions leading to hemolysis and platelet aggregation. To simplify the complexity of the project, the following assumptions have been made:

1. Inlet flow is through a straight, rigid, circular tube.
2. No-slip boundary condition.
3. Flow is fully developed.
4. Fluid is Newtonian.
5. No wave reflection in pulsatile flow.

These assumptions will be applied throughout the rest of this chapter in developing the principal equations.

3.1 Steady Flow in a Tube

Flow through a tube is governed by the Navier-Stokes (N-S) equations and the equation of continuity. By applying the aforementioned assumptions and eliminating negligible terms in the N-S equations, flow through the shunt can be described by the following equation:

$$\rho \frac{\partial u}{\partial t} + \frac{\partial P}{\partial x} = \mu \left(\frac{\partial^2 u}{\partial^2 r} + \frac{1}{r} \frac{\partial u}{\partial r} \right) \tag{3.1}$$

This is the highly simplified form of the governing equation on which solutions for fully developed steady and pulsatile flow are based [17]. Since the pressure force driving the flow is constant and not a function of time, the velocity is also independent of time, and the equation can be reduced to:

$$\frac{dP_s}{dx} \;=\; \mu\,(\frac{\partial^2 u_s}{\partial^2 r} \;+\; \frac{1}{r}\;\frac{\partial u_s}{\partial r}\;) \tag{3.2}$$

Applying the no-slip boundary condition and constant maximum velocity at the center of the tube, the solution for flow now becomes:

$$u_s \;=\; \frac{k_s}{4\mu}\,(r^2 \;-\; a^2) \tag{3.3}$$

where k_s is the constant pressure gradient and a is the radius of the tube. This is the equation for steady Poiseuille flow in a cylindrical tube [17].

The velocity profile in steady fully developed *Poiseuille flow* is parabolic in shape where velocity is zero at the walls and maximum at the center of the tube. The profile is such that the mean velocity is half the maximum velocity. The velocity profile can be non-dimensionalized in terms of the maximum velocity by applying the condition to Equation 3.3 that at r = 0, velocity is a maximum (u_{max}):

$$\frac{u_s(r)}{u_{max}} \;=\; 1 \;-\; (\frac{r}{a})^2 \tag{3.4}$$

One of the fundamental properties and important reasons for this study is the rate of deformation of the fluid. If the radial and angular velocities are considered to be zero in *Poiseuille flow*, then the relation between shear stress (τ) and the rate of shear (du/dr) is simply:

$$\tau_{xr} \;=\; \mu\;\frac{du}{dr} \tag{3.5}$$

If radial velocities are not considered to be zero, then another component to consider is vorticity. Vorticity is associated with rigid body rotation of a particle about some fixed point, where the orientation of the particle changes during the rotation. It is related to the shear across the particle, and is determined by the following equation:

$$Vorticity \;=\; \frac{dv}{dx} \;-\; \frac{du}{dr} \tag{3.6}$$

3.1.1 Entry Length

Poiseuille flow is an idealized flow based on the assumption that the tube is infinitely long so that flow is not affected by the tubes entrance. In the cardiovascular system, flow is often through short segments, as in an SPA shunt. The flow through these tubes or segments does not reach fully developed *Poiseuille flow* because the entry length is greater than the length of the tube. For uniform flow, the entry length, L_e, is defined as

$$L_e \;=\; (0.04\ Re)\ d \tag{3.7}$$

where Re is the dimensionless Reynolds number [17]. The length of an SPA shunt used in the Norwood procedure varies slightly between infants, but on average is 15 mm long. So for a 3.5 mm shunt, with a Re of roughly 1200, the length required to reach fully developed flow is 16.8 cm (168 mm). Thus, under *in vivo* conditions, flow through a shunt is not fully developed, and entrance and exit effects are present.

3.1.2 Flow Seperation

Flow separation occurs when the pressure in the flow field increases in the direction of the flow. The flow separates due to the presence of an adverse pressure gradient. The adverse pressure gradient can generate a backflow against the boundary layer, deflecting the boundary layer off the surface. This separation point moves downstream if the adverse pressure gradient is weaker and upstream if the gradient is stronger. In the case of an adjustable shunt, separation of flow can occur after the constriction where flow first accelerates and then decelerates. Clinically, this is important because flow separation indicates areas of flow reversal and low flow, which could increase the risk of plaque build-up and thrombosis.

3.2 Pulsatile Flow in a Tube

Flow in a tube in which the driving pressure varies in time was given in Equation 3.1. For pulsatile flow, this pressure is oscillatory in time, and becomes a function of both distance (x) and time (t) as shown by the following equation:

$$\frac{dP}{dx} \;=\; k_s e^{iwt} \;=\; k_s(\cos wt \;+\; \sin wt) \tag{3.8}$$

where k_s is the amplitude of the oscillatory pressure gradient and ω is the frequency of oscillations. A typical composite pressure waveform produced by the heart is shown in Figure 3.2. Substituting

this equation back into Equation 3.1 yields:

$$\frac{\partial^2 u_\phi}{\partial r^2} + \frac{1}{r}\frac{\partial u_\phi}{\partial r} - \frac{\rho}{\mu}\frac{\partial u_\phi}{\partial t} = \frac{k_s}{\mu}e^{iwt} \tag{3.9}$$

This complex equation is very difficult to solve. However, it is known that

$$u_\phi(r,t) = u_\phi(r)e^{iwt} \tag{3.10}$$

Substituting this into Equation 3.11 cancels out the factor e^{iwt}, leaving an ordinary differential equation:

$$\frac{d^2 u_\phi}{dr^2} + \frac{1}{r}\frac{du_\phi}{dr} - \frac{i\alpha^2}{a^2}u_\phi = \frac{k_s}{\mu} \tag{3.11}$$

This equation is now a form of Bessel equation that has a known general solution, where the term α, called the Womersley number, is given by:

$$\alpha = a\sqrt{\frac{\rho\omega}{\mu}} \tag{3.12}$$

The Womersley number is an important dimensionless parameter that may be thought of as an oscillatory Reynolds number. For two different pulsatile flow systems to have the same velocity profiles and exhibit the same physical characteristics, they must not only have the same Re, as in steady flow, but must also match α.

Small α values result in quasi-steady flow with oscillatory parabolic velocity profiles. In fact, at very low frequencies, the relationship between pressure and flow becomes the same as in steady *Poiseuille* flow. For large values of α, or high frequency oscillations, the flow is unable to keep pace with the changing pressure. This results in the flow reaching less than the fully developed *Poiseuille* flow profile at the peak of each cycle. The higher the frequency, the lower the peak velocity. The velocity profiles for different values of α are shown in Figure 3.1 [17] [19].

3.3 Characteristics of Blood

Blood is an extremely complex, non-Newtonian fluid in which the viscosity changes as shear rate changes. This is in part due to the presence of red blood cells (RBCs), which can form aggregates known as rouleaux that occur in areas of low flow, or low shear rate. Blood at normal hematocrit and low shear rate is commonly modeled as a Casson fluid with a certain yield stress and a shear-rate dependant apparent viscosity. However, at shear rates grater than 100 s^{-1}, blood has been shown to behave as a Newtonian fluid. Large increases in shear rate above 100 s^{-1} produce

small changes in the apparent viscosity [20]. Thus, although blood is non-Newtonian, it is modeled as a Newtonian fluid with a constant apparent viscosity throughout this study. This assumption has also proved to be adequate when the tube diameter is large in comparison to capillaries and other tiny blood vessels in the arterial tree [17].

As mentioned in Chapter 1, damage to these blood cells due to high shear stresses is a major concern. Although there has been very little quantitative *in vivo* information regarding maximum shear stresses leading to damage of RBCs and platelets, extensive *in vitro* experiments have been performed estimating the maximum limits of allowable shear stress in blood. Assessing the potential damage to RBCs (hemolysis) and platelets has been shown to be a function of both the shear stress field and the duration of exposure of the blood cell to the stress field [21].

3.3.1 Hemolysis

Tearing or ripping of RBC's has been shown to occur when cells are exposed to excessive shear or turbulence in the circulation. This form of mechanical injury, known as hemolysis, is important in the clinical setting as it can lead to severe anemia and even heart failure. Wurzinger, using a viscometer, observed hemolysis at laminar shear stresses of 255 N/m^2 (2550 $dynes/cm^2$) with an exposure time of 700 ms [22]. Another study conducted by Sallam and Hwang using a one-component laser Doppler anemometer found the threshold for hemolysis in turbulent flow to be 400 N/m^2 (4000 $dynes/cm^2$) for an exposure time of 1 ms [23]. However, probably a greater concern than damage to RBCs is shear-induced platelet aggregation (SIPA) [21].

3.3.2 Shear-Induced Platelet Aggregation

Platelets contain a series of subcomponents that interact with proteins in the bloodstream. Platelet aggregation induced by high shear stress is mediated by von Willebrand factor (VWF), a large protein that enables platelets to adhere to exposed subendothelium [24]. Shear forces increase the adhesiveness of VWF, which uncoils its three-dimensional (3D) globular shape in the direction of the shear stress field. Increased amounts of VWF have been observed in neonates up to the age of 8 weeks, and studies using neonatal plasma have shown increased platelet deposition on the subendothelium in the presence of high shear stress [25].

Several studies using a cone and plate viscometer have demonstrated that high fluid shear stress at levels similar to those experienced by platelets at the throat of a stenosis could induce platelet activation and aggregation [4]. Anderson *et al.* [26] studied the effects of shear stress on platelets in human platelet-rich plasma (PRP) using a rotational viscometer, and found that for a 5

minute exposure time, shear stresses above 160 dynes/cm^2 induced platelet lysis. For an exposure time of 30 seconds, platelets could sustain shear stress levels up to 600 dynes/cm^2 before lysis.

One problem with these *in vitro* studies is that the time of exposure to the stress fields is significantly longer than what platelets would experience through a stenosis, as in the case of this project [26]. In addition, the flow dynamics through the constriction is not only a high shear environment, like most studies, but combinations of high and low shear flow fields. Low shear rates and flow stasis on the intimal surface of grafts have been shown to play an important role in local thrombus formation. Thrombi may detach from a surface and be carried downstream, eventually occluding a blood vessel and impairing blood flow [28]. Unfortunately, few studies have investigated the role of low shear stress on platelet adhesion, and so the effects of slow flow and recirculation regions on blood remains largely unknown [4].

Zhang *et al.* [4], however, investigated platelet aggregation and activation under a complex pattern of shear stress in which platelets were exposed to a brief pulse of high shear followed immediately by a region of low flow. This allows for evaluation of SIPA in a more physiological environment, as would be seen in an adjustable SPA shunt. A computerized viscometer was used to create a constant high shear stress for a specified amount of time followed immediately by a period of low flow. Zhang found that platelet aggregation can occur when platelets are exposed to a shear stress of 100 dynes/cm^2 for a short period of 2.5 seconds.

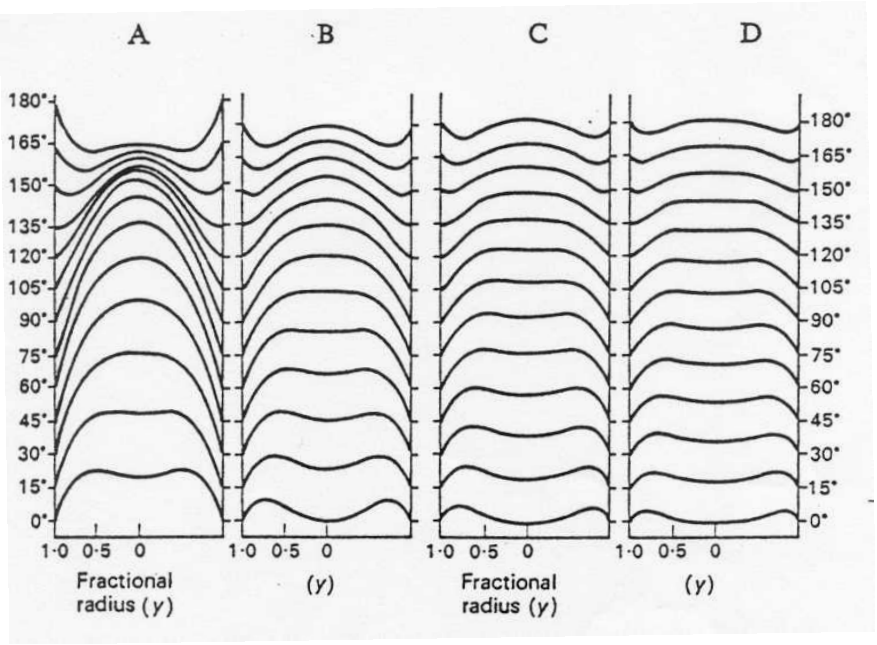

Figure 3.1: Velocity profiles of oscillatory flow in a pipe with varying α. Values of α are 3.34(A), 4.72(B), 5.78(C), and 6.67(D) [19].

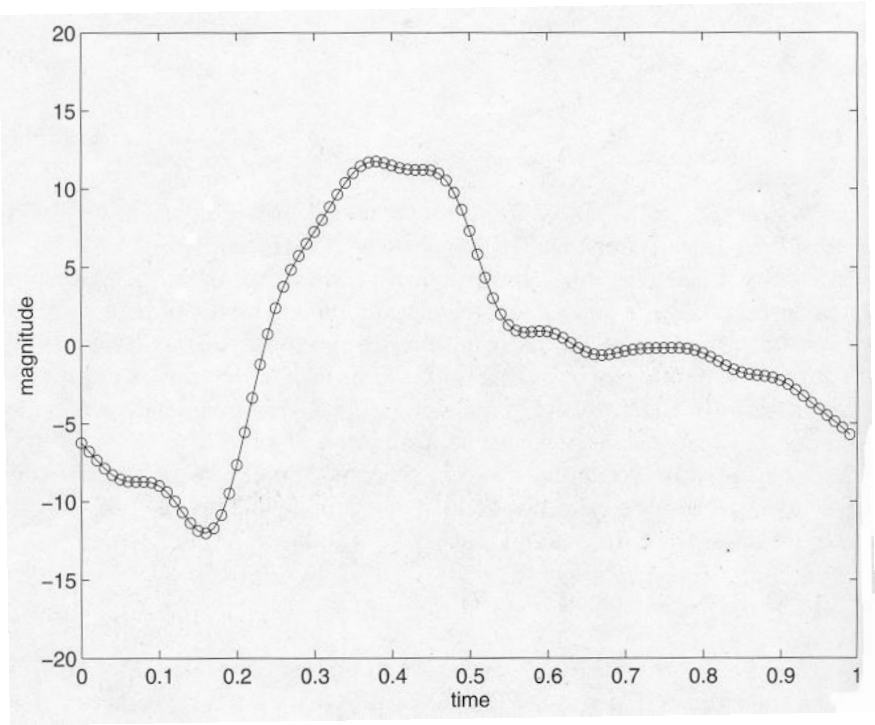

Figure 3.2: Typical composite pressure waveform produced by the heart [17].

Chapter 4

Experimental Setup

4.1 Part 1: Creating Optically Clear Flow Models

4.1.1 Mock Arterial Circulatory System

The first part of this chapter details the steps for creation of the phantom flow models used for *in vitro* testing. A flow circuit was first created to mimic that of an infant's arterial circulatory system. A complete schematic of the closed flow system is shown in Figure 4.1. The flow circuit includes a steady flow fountain pump, two pressure gauges, two electromagnetic flow probes with a Zepeda Instruments dual channel flow meter, flow resistor clamps, a reservoir, tygon tubing, tube couplings, two 3-way valves, and two pairs of Plexiglas tubes measuring 4" in length. The National Instruments Labview program Biobench was used for data acquisition after appropriate calibrations.

Mean flow rate through the shunt was shown to be independant of pulse pressure, and only dependant upon the mean shunt inlet and outlet pressures. Thus, the mean shunt flow rate is the same under both steady flow and pulsatile flow conditions, as long as the mean pressure drop across the shunt is held constant. The investigation can be seen in further detail in Appendix A. These results agree with previous studies that have demonstrated that with a constant pressure drop across a shunt, steady flow is a good approximation of mean cardiac flow [27]. Therefore, the initial part of the study was conducted using only a steady flow pump.

The pump, representing the heart, had a flow rate of approximately 10 L/min. Since this was much greater than needed, part of the output from the pump was diverted in a controlled method back into the reservoir using a Y connector and a flow resistor clamp (not shown in Figure 4.1. The Plexiglas tubes measured 7 mm in diameter and had a metal connector on one side used for

easy insertion and removal of a shunt. These replaced the need for sutures. Pressure taps were placed in the Plexiglas tubes across from the metal connectors to measure inlet and outlet shunt pressures.

The flow rate through the entire flow circuit was measured with a flow meter placed proximal to the shunt. Shunt flow was measured with a flow probe placed in the pulmonary circulation. Adjustable resistor clamps were placed in the flow circuit to control shunt inlet pressure (by adjusting systemic vascular resistance) and outlet pressure (by adjusting pulmonary vascular resistance). In this manner, inlet and outlet pressures were controlled independently. All output from the arterial and pulmonary circulations fed back into a large reservoir directly feeding the pump. The fluid in the flow circuit consisted of 64.5% water and 35.5% glycerin, which yields a viscosity of approximately 3.3 centipoise (cp). The solution approximates the viscosity of blood at body temperature.

4.1.2 Creating constricted shunts

As mentioned in Chapter 1, shunts of 3.5 mm in size are most commonly used in neonates suffering from HLHS. Although a 3.5 mm shunt may not always provide optimal pulmonary flow, larger sized shunts (4 mm and 5 mm) present a greater risk in excessive pulmonary blood flow. Since these sized shunts will be the initial target of an adjustable SPA shunt, both a 4 mm and a 5 mm shunt were constricted to match the flow rate of an open 3.5 mm shunt.

After assembling the mock flow circuit, a 3.5 mm shunt was placed between the Plexiglas tubes, joining the systemic and pulmonary circulations. The pump was activated and systemic and pulmonary vascular resistance were adjusted using the resistor clamps until shunt inlet and outlet pressures were 50 mmHg and 20 mmHg as seen *in vivo* [29]. The flow probes were calibrated by altering flow with the 3-way valves and using a beaker and a stop watch. Once the flow meters were calibrated and the system stabilized with constant inlet and outlet pressures of 50 mmHg and 20 mmHg, respectively, the flow rate through the open 3.5 mm shunt was recorded. The trial was repeated five times. Once the average flow rate through a 3.5 mm shunt was established, the prototype of a 4 mm adjustable shunt, shown in Figure 4.2, was placed in the mock flow circuit and constricted so that the flow rate matched that of the 3.5 mm shunt. The constricted 4 mm shunt, still inside the housing, was then detached from the flow system and replaced with a 5 mm shunt, and the process repeated. The average flow rates through the 3.5 mm, 4 mm, and 5 mm shunts before and after constriction are given in Table I.

4.1.3 Image Acquisition and Processing

Once the 4 mm and 5 mm adjustable shunts were constricted and removed from the flow circuit, they were filled with vinyl polysiloxane impression material (Reprosil). The impression material, (1:1 ratio of base and catalyst), was injected into the lumen of the constricted shunts with a 10 cc syringe. The molding was allowed to harden for 24 hours before the plunger was detached and the shunt removed from the housing. The shunt was then placed in a contrasting blackened wax cast on top of an aluminum base. A small hole, used as a fiducial mark, was drilled parallel to the shunt through the wax and injected with 5μ polystyrene particles (Moncanto Co., Ohio) (Figure 4.3).

Next, the aluminum base was fastened to the platform of a PMV microtome and several cuts, ranging in number from 35 to 45 slices depending upon the length of the shunt, were made perpendicular to the shunts long axis. The thickness of each slice or cut was 0.35 mm. A Dage MTI Series 68 monochrome video camera fixed atop the cutting blade arm captured an image of the cross-section of the graft after each slice. The software QuantIm (ZEDEC) was used for image acquisition and processing, allowing real time feedback from the camera. The following steps outline the method used in this processing technique:

1. Images of the cross-section of the graft were captured after each cut with a slice depth of 0.35 mm. Figure 4.4 shows a series of cross-sectional images through the throat of a constricted 4 mm shunt.

2. The images were aligned in QuantIm using the small fiducial mark.

3. The lumen of the shunt was outlined using QuantIm and saved as a series of (x,y) coordinates in a text file.

The written script files used for image acquisition and processing in QuantIm can be seen in Appendix B.

4.1.4 3-D Computer Generated Modeling

MATLAB was first used to format the QuantIm text files, adding a z-coordinate representing the depth of each cross-section, and creating a necessary file containing a path line used to join all the cross-sections. The code for MATLAB program can be seen in Appendix C. The cross-sectional geometry of each image was then imported into I-DEAS (Electronic Data Systems, TX), a 3-D CAD package (Figure 4.5). The path line formed in MATLAB was used in lofting all the cross-sections together, creating a solid. As previously mentioned, the asymmetric constriction was

compared with an ideal axisymmetric constriction. Figure 4.6 shows the CAD model of a 4 mm constricted shunt and an equivalent axisymmetric constriction, which was modeled by matching the cross-sectional area through the throat.

4.1.5 Forming optically clear models

Stereolithography (SLA) models were next made from the computer generated shunts. From these SLA models, optically clear glass tubes were shaped to match the constriction of the SLA parts. Both asymmetric and axisymmetric glass models measuring 0.5" in inner diameter were formed for each shunt. These models were used evaluate the differences between the two types of constriction. An asymmetric 4 mm shunt showing both the SLA and final glass model can be seen in Figure 4.7.

After establishing a relationship between an ideal axisymmetric and the actual asymmetric constriction, additional flow models of the 4 mm and 5 mm shunts were created in order to match both dimensionless parameters for *in vitro* testing. These models were scaled smaller in diameter in order to match both Re and α due to limitations of the pumps output. To ensure the models closely matched the actual constricted shunts, SLA plates were created from 3-D CAD models and used as tools to shape acrylic tubes. The tubes measured 0.25" in inner diameter, and were chosen due to the forming temperature of acrylic (270^oF). This temperature was well below the melting temperature of the SLA resin. The top plate was designed with a slot containing the inverse of the constriction. The bottom plate was used to hold the heated acrylic tube in place while the top plate pressed the constriction into the tube. The acrylic tubes were heated with a heat gun for 2-3 minutes before being pressed.

4.2 Part 2: *In Vitro* Testing using Particle Image Velocimetry

4.2.1 Particle Image Velocimetry (PIV)

PIV and its digital counterpart, DPIV (digital particle image velocimetry), are techniques for extracting instantaneous velocities in two or more dimensions. DPIV is a relatively new variation of the classical PIV method that was notorious for being extremely tedious and required exhaustive setup requirements making it too impractical for use. DPIV makes use of modern imaging and computational hardware to greatly reduce the difficulty of extracting valuable measurements [31]. DPIV works by illuminating a seeded flow field using a laser light sheet. The resultant planar images are digitally recorded using a charge-coupled device (CCD) camera. Successive images are computationally analyzed by taking numerous sub-regions and determining the movement of particles within the regions via fast Fourier transforms (FFT). Using the timing between the images, the planar velocities throughout can be determined. This availability of instantaneous 2-D flow field data (x-y velocities in a plane over time) gives great insight about spatial and temporal details of the flow physics and can be used to study flow or for computational validation. It has been shown to be useful for in *in vitro* studies [32] and recent advances even suggest that *in vivo* DPIV measurements may be possible in the near future using high speed ultrasound equipment [33].

A schematic of the PIV flow system is shown in Figure 4.8. A 25 mJ double-pulsed Nd:YAG laser was used as the light source. Configuration and alignment of three biconcave lenses was used to adjust the light sheet to the desired thickness and width. The goal is to achieve a very thin, horizontal sheet of light in the desired area of visualization. The fluid was seeded with 40 micron silver-coated hollow glass spheres which serve as the tracer particles when illuminated. The motion of the tracer particles was captured using a 10-bit dual channel Kodak MegaPlus ES:1.0 monochrome CCD camera (Figure 4.9). The frame grabber/camera combination has a double trigger feature that allows two images to be acquired back-to-back within a given time (1μs-1ms). The delay between the laser pulses, and thus the time between successive images, can be adjusted with the use of a timing box and an oscilloscope, and is dependant upon the speed of flow. Longer delays in high speed flows may result in particles traveling outside the examined window area, while short delays in low speed flows may lead to overlap of the particles within the same window from one image to the next. For a detailed discussion of particle motion in a fluid and determination of the velocity components, refer to Roclawski [34]. For comparison between axisymmetric and asymmetric tubes, a total of 62 image pairs were recorded for each PIV run, while 128 image pairs were recorded for each PIV run matching Re and α for the 4 mm and 5 mm shunts. The images

were processed using a wall adaptive Lagrangian parcel tracking (WALPT) algorithm developed by Sholl and Savas [35]. The window size used in the processing was 32x32 pixels.

4.2.2 Experimental Parameters

The axisymmetric and asymmetric constricted models, paired together by matching the cross-sectional area through the throat, were tested under both pulsatile and steady-flow conditions. A Harvard Instruments hydraulic pulsatile pump was used to create oscillatory flow in the circuit. The frequency of the pump was set such that 70% of the cycle was spent in diastole, or refilling, and 30% in systole, or pumping, similar to average *in vivo* conditions. Each model was placed inside a water-filled glass box to correct for image distortion at the walls of the tube. Data was collected at three different locations: upstream, throat, and downstream. Table 4.2 gives the Re and α for *in vivo* conditions and for the *in vitro* PIV flow circuit. Table 4.3 lists the properties of both water and blood used in the calculations. All of the experiments were conducted at room temperature (23^oC).

As previoulsy stated, these runs did not match α as seen *in vivo* due to limitations on the maximum output of the pulsatile pump. Table 4.4 shows the frequency and stroke volume settings on the pump required to match the *in vivo* dimensionless numbers for the smaller 0.25" diameter models. Data for these models were collected at four different regions within the models: (1) upstream of the throat, (2) at the throat, (3) 0-2 diameters downstream of the throat, and (4) 2-4 diameters downstream of the throat. Flow through an open 3.5 mm shunt at one location was also collected. One problem with the flow system was that the pulsatile pump and the laser/camera combination were not synchronized. Therefore, enough image pairs had to be captured through one complete cycle to ensure that the results obtained from PIV included values very close to peak systolic values. Based upon the frequency of the laser/camera and the frequency of the pulsatile pump, approximately 21 image pairs (measurements) were captured for each cylce of flow through a 4 mm shunt. For a 5 mm shunt, approximately 13 image pairs were taken per pulse cycle. An illustration of these of data points collected over a typical pressure waveform that might be produced by the heart is shown in Figure 4.10. Since the camera and pump were not sychronized, these data points would be slightly shifted in successive cycles.

Shunt Size (mm)	Flow Rate (cc/min)	
	Open	Constricted
3.5	600	-
4.0	650	600
5.0	720	600

Table 4.1: Flow rates through 3.5 mm, 4.0 mm, and 5.0 mm shunts.

in vivo Conditions						
Shunt Size (mm)	Inner Diameter (mm)	Heart Rate (beats/min)	Stroke Volume (cc)	Flow Rate (cc/min)	Re	α
4.0	4.0	120	5	600	1061	4.09
5.0	5.0	120	5	600	849	5.12
in vitro Conditions						
Shunt Size (mm)	Inner Diameter (mm)	Heart Rate (beats/min)	Stroke Volume (cc)	Flow Rate (cc/min)	Re	α
4.0	12.7	120	5	600	1061	23.14
5.0	12.7	120	5	600	1061	23.14

Table 4.2: *In vivo* and *in vitro* parameters

Property		Blood	Water
ρ	kg/m^3	1051	998
μ	centipoise	3.2	0.994
ν	centistoke	3.0	0.946

Table 4.3: Physical properties of blood and water

3.5 mm SPA Shunt						
	Diameter (mm)	Frequency (beats/min)	Stroke Volume (cc)	Flow Rate (cc/min)	*Re*	α
In vivo	3.5	120	5	600	1213	3.58
Flow Circuit	6.35	11.5	30	343	1213	3.58
4 mm SPA Shunt						
	Diameter (mm)	Frequency (beats/min)	Stroke Volume (cc)	Flow Rate (cc/min)	*Re*	α
In vivo	4.0	120	5	600	1061	4.09
Flow Circuit	6.35	15	20	300	1061	4.09
5 mm SPA Shunt						
	Diameter (mm)	Frequency (beats/min)	Stroke Volume (cc)	Flow Rate (cc/min)	*Re*	α
In vivo	5.0	120	5	600	849	5.12
Flow Circuit	6.35	23.5	10.2	240	849	5.12

Table 4.4: Parameters necessary for matching Re and α

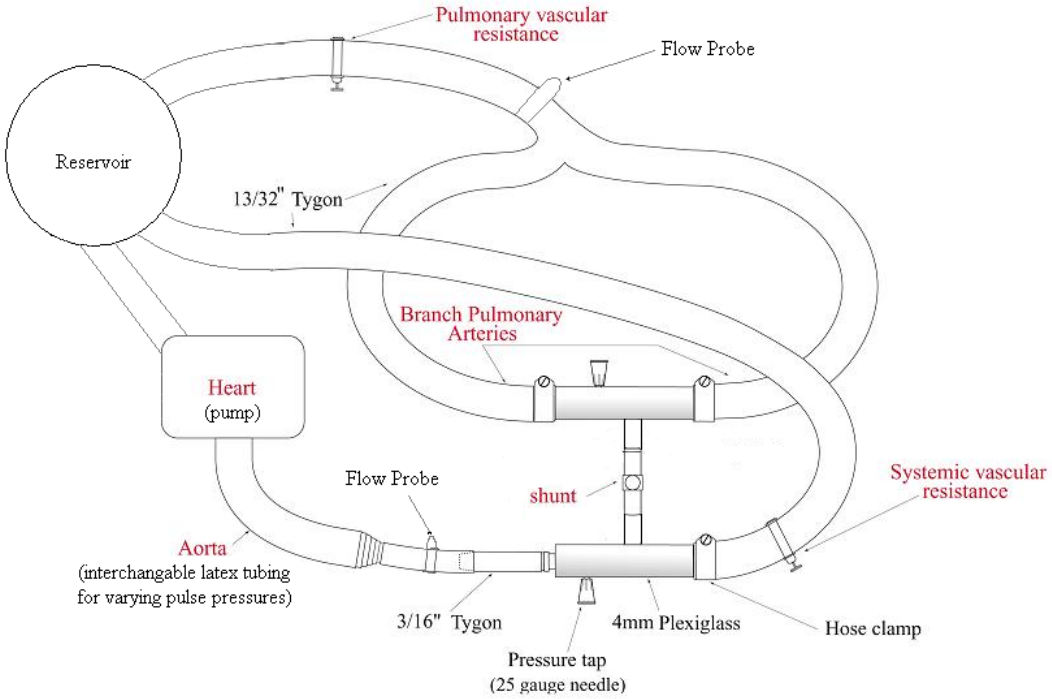

Figure 4.1: Mock flow circuit of an infant's arterial circulatory system. Shunt connects systemic and pulmonary circulation.

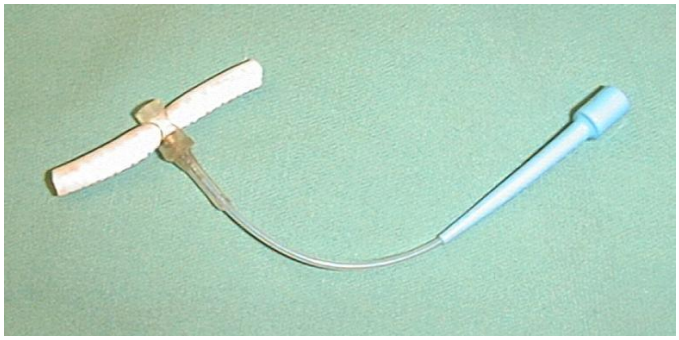

Figure 4.2: Prototype of the actual 4 mm adjustable SPA shunt used in the study.

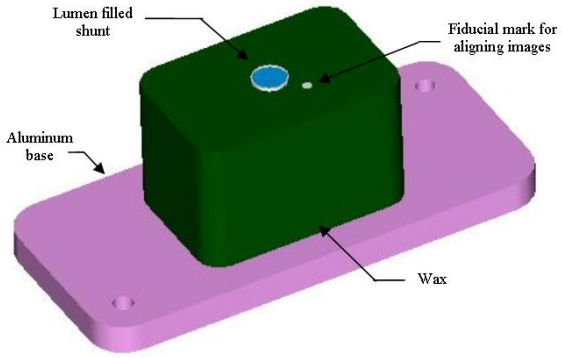

Figure 4.3: Wax cast used to hold shunt during slicing. Fiducial mark used for alignment of images during processing.

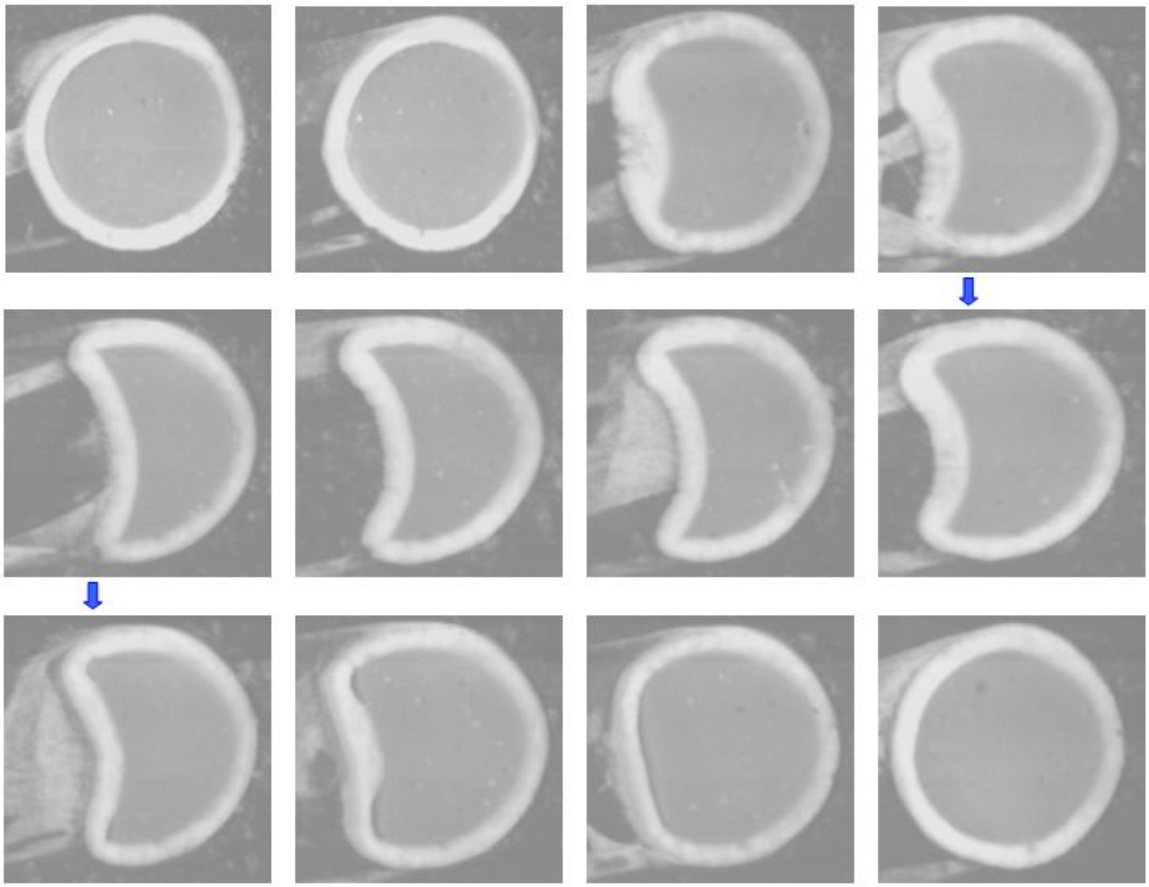

Figure 4.4: Series of cross-sectional images through the throat of a constricted 4 mm shunt (left to right). Distance between images ranges from 0.70 mm - 1.05 mm.

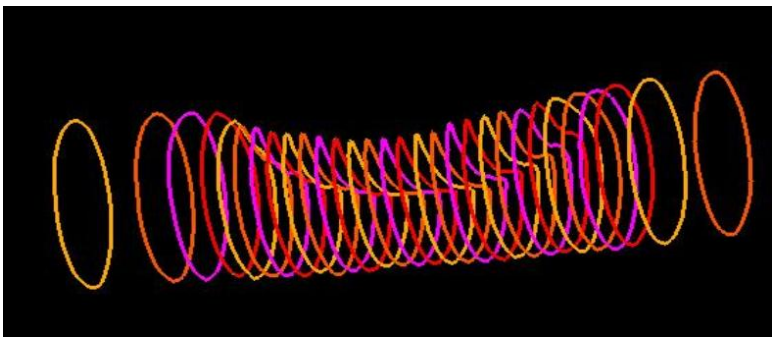

Figure 4.5: Cross-sectional geometry of each image.

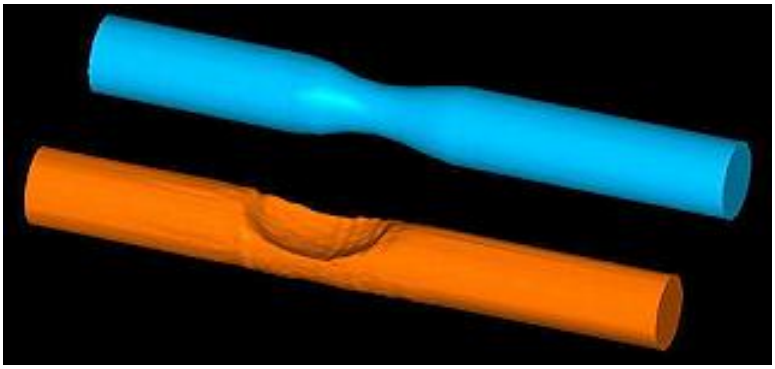

Figure 4.6: CAD models of an asymmetric and axisymmetric constriction within a 4 mm shunt.

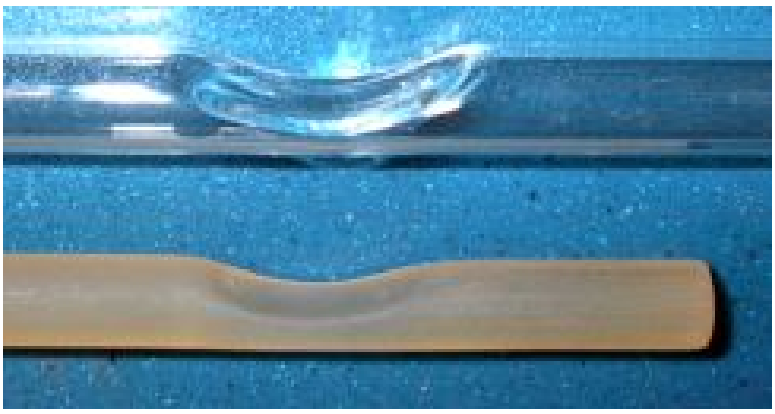

Figure 4.7: SLA and glass model of a 4 mm shunt.

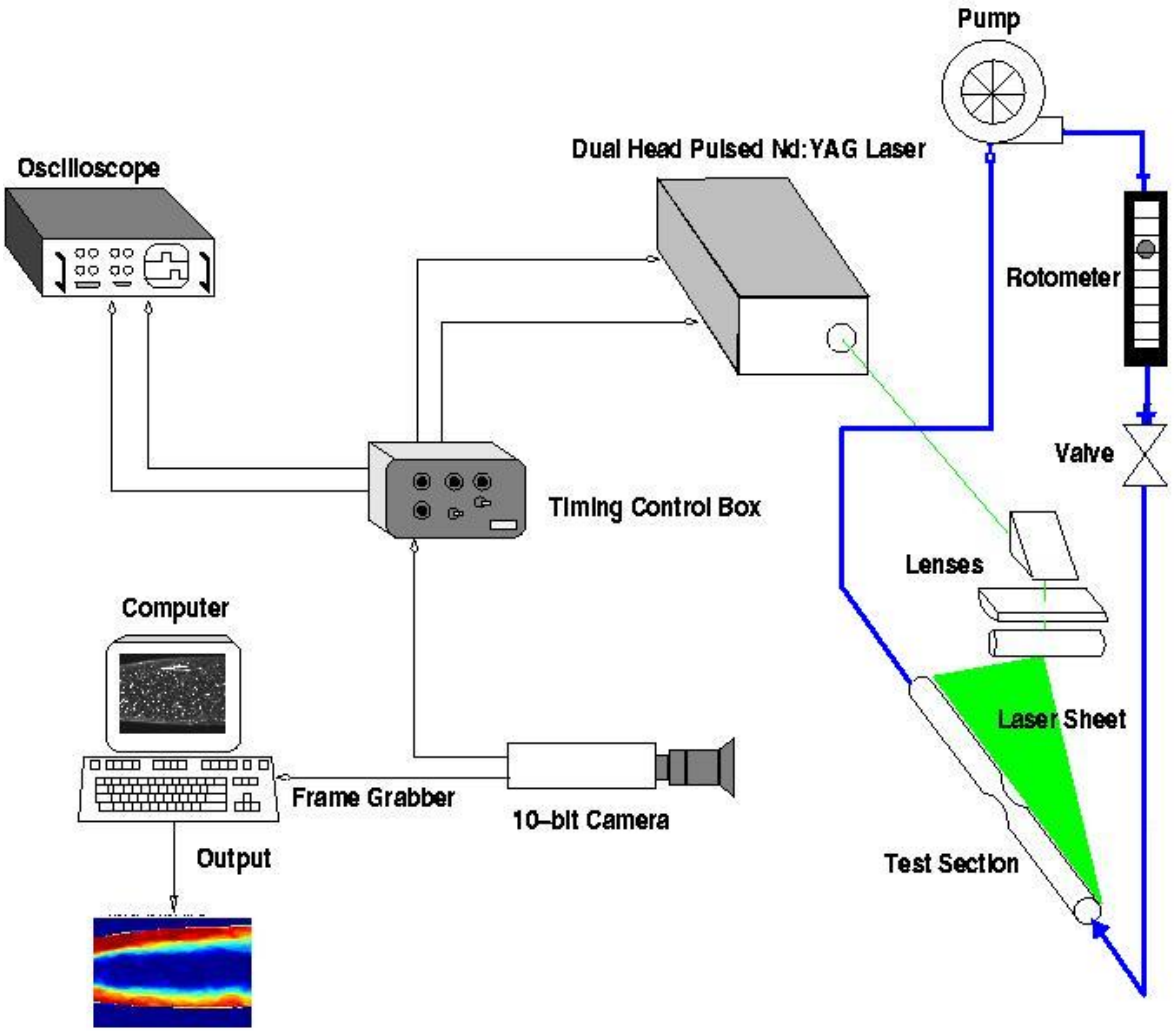

Figure 4.8: Schematic of the PIV flow circuit.

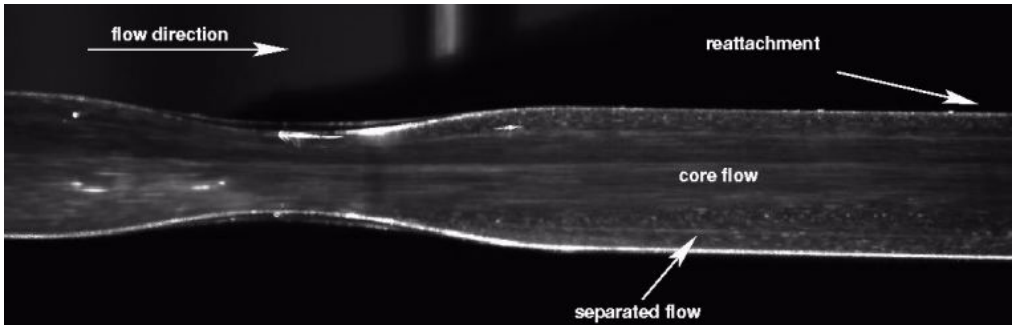

Figure 4.9: Raw image from PIV showing areas of high particle velocity and separation of flow downstream of the constriction.

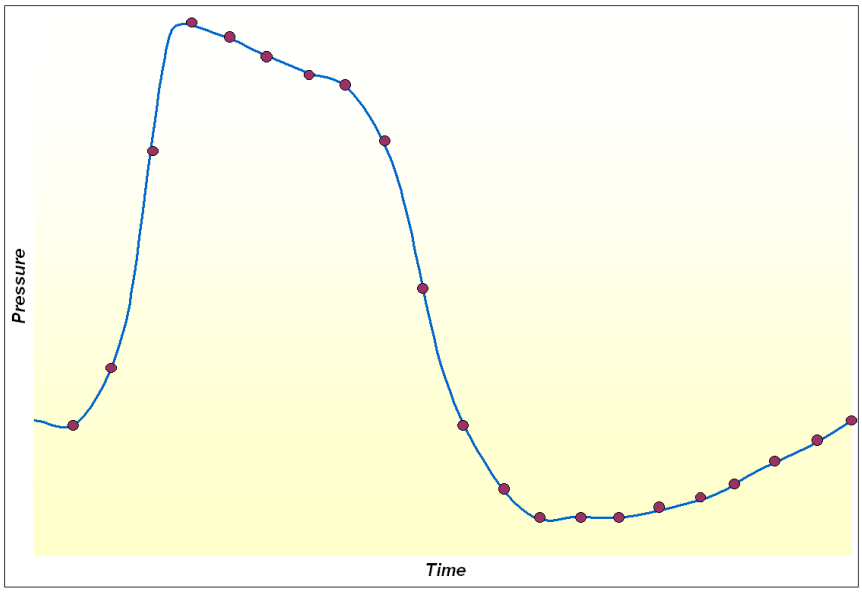

(a)

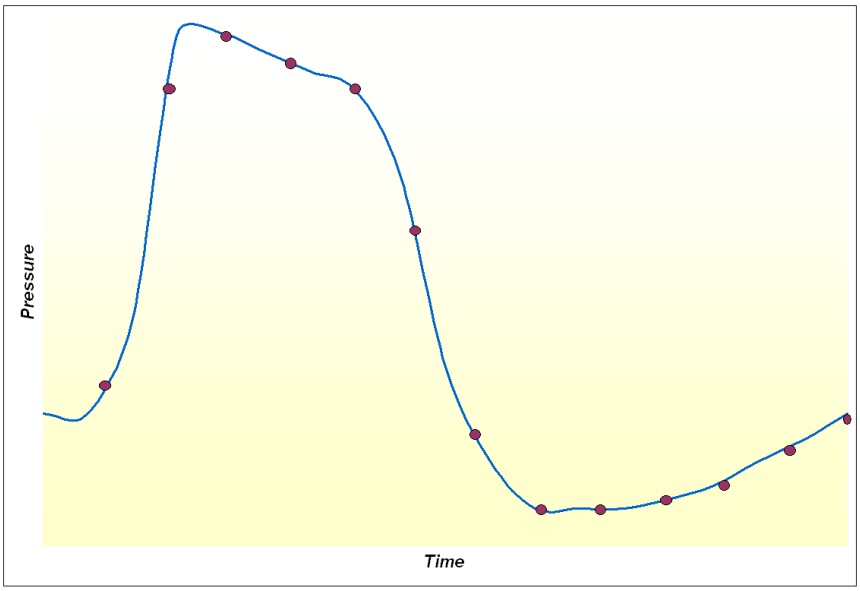

(b)

Figure 4.10: Number of PIV measurements taken through each complete pulse cycle in (a) a 4 mm shunt and (b) a 5 mm shunt. Pressure pulse is simulated for illustrative purposes only.

Chapter 5

Results

5.1 Post-Processing

Once the PIV images were captured for all flow tests through the different tubes, one image from each run was analyzed in XCAP, the frame grabber software. This was necessary to outline the area of flow through the shunts on the images, creating a mask file. The 10-bit mask was then coverted into an 8-bit binary image using MATLAB. Input files were created for each run and, along with the 8-bit binary image, were used by the WALPT algorithm in processing the raw images. The output from the algorithm are binary files containing the velocity vector (u,v) and its gradient tensor,

$$u_{ij} = \begin{pmatrix} \partial u/\partial x & \partial u/\partial y \\ \partial v/\partial x & \partial v/\partial y \end{pmatrix}$$

at each point.

The velocity vectors and shear rates were then extracted from the binary tensor files using another MATLAB routine. This script file can be used to calculate quantities such as vorticity, reverse flow probability (RFP), shear stresses, skin friction, and velocity profiles. RFP is simply the percent of time that flow is in the opposite direction. Examples of some of the MATLAB script files used for post-processing can be found in Appendix C. Multiple sets of data were also collected at each location within the flow models. Figureinclude figure shows the RFP under pulsatile flow conditions in a 4 mm shunt for 128 image pairs collected during the first trial. Figureinclude girue shows the RFP in the same 4 mm shunt at the same location for another 128 image pairs collected after the flow system was turned off and restarted. The two RFP fields are almost identical in size and value, which shows reproducability between the test cases, and validates the experimental results. This is especially important for pulsatile flow, since the camera/laser and pump were not

synchronized.

The first part of this chapter presents the results of a comparison between the two different types of constriction, axisymmetric and asymmetric. The second part involves an in-depth look at an asymmetric constriction matching *in vivo* dimensionless parameters.

5.2 Asymmetric vs. Axisymmetric Constriction in an Adjustable SPA Shunt

The main focus for evaluating the two different forms of constriction is primarily on comparing RFP and maximum average vorticities and velocities. The maximum values for average velocity (V_{MAX}), average vorticity, and reattachment length (L_R) for a 4 mm shunt model under both asymmetric and axisymmetric constriction are shown in Table 5.1, where L_R indicates the distance downstream of the throat that reverse flow is observed. These results are for steady flow and pulsatile flow conditions matching *Re* of 1061 (α=23.14, but was not matched). The values provided in the table are based upon the average over one cycle, not the absolute maximum that would be seen during peak oscillatory flow. When compared to an ideal axisymmetric constriction in a 4 mm shunt, maximum values of velocity and vorticity are higher in the asymmetrically constricted model. In fact, maximum vorticity increases 22%-35% in an asymmetric constriction depending upon the type of flow. In addition, areas of flow reversal can be seen downstream of the throat for the asymmetric constriction for both steady and pulsatile flow, while no seperation of flow is observed in the axisymmetric constriction. The length of flow seperation is also much less under pulsatile flow for teh asymmetric case and non-existent for teh axisymmetric model.

Similar results are confirmed for a constricted 5 mm shunt, as shown in Table 5.2. The difference, however, in vorticity under pulsatile flow in the two constrictions appears to be minimal. Unlike the 4 mm shunt, regions of flow separation are observed for the axisymmetrically constricted 5 mm shunt. It should also be pointed out that maximum values of average velocity and vorticity are less for pulsatile flow than steady flow in both shunts. This will be addressed in the subsequent chapter.

Plots detailing the velocity field, vorticity, and reverse flow probability (RFP) downstream of the constriction can be seen in Figure 5.2 through Figure 5.5. For pulsatile flow, these results show the average over a complete pulsatile cycle. Vorticity is highest in the models through the throat and along the top wall just distal to the throat. The colorbar provided in each image assigns a numerical value to the color gradient shown for RFP, where red indicates the highest areas of

reverse flow and blue indicates areas of little or no reverse flow. In steady flow, the shear layer has regions of reversed flow near the wall distal to the throat resulting in eddy formation. The shedding of vortices is observed for steady flow in a 5 mm shunt as far as 3 diameters downstream of the constriction where the RFP is around 50%. A graphical representation of flow reversal along the bottom wall of the shunt is given in Figure 5.10.

Velocity profiles proximal and distal to the throat for pulsatile flow in both the 4 mm and 5 mm models can be seen in Figure 5.6 and 5.7. The time interval between profiles is approximately 0.1 seconds. The velocity profiles in both the 4 mm and 5 mm models prior to the throat are identical, with a blunt profile shape rather than parabolic. However, the velocity profiles are different downstream of the constriction, where reverse flow is much greater in the 5 mm model.

5.3 Asymmetric Constriction Matching Both Re and α

Once the relationship between an axisymmetric constriction and an asymmetric constriction was established, results were then obtained detailing actual values of velocity, shear rate, vorticity, and RFP as seen *in vivo* through both a 4 mm and 5 mm adjustable SPA shunt by matching the dimensionless parameters (Table 4.4). The maximum average vorticity and velocity in two different regions distal to the throat are shown in Table 5.3. Higher values of maximum velocity and vorticity exist in a 5 mm shunt immediately post-stenosis, as would be expected. However, values for velocity and vorticity 2-4 diameters downstream of the constriction are similar in the two shunts.

One area of interest is the maximum value of shear rate seen in both shunts during systole. Table 5.4 shows the maximum values of shear rate and shear stress during systole in a 3.5 mm, 4 mm, and 5 mm shunt. The shear stress was calculated based upon the properties of blood in Table 4.3. As expected, much larger values of maximum shear rate are seen in the constricted models as opposed to a wide open 3.5 mm shunt.

The differences in these peak values between the 4 mm and 5 mm models, though, is smaller than anticipated, leading to initial assumptions that the flow fields might be similar. However, the L_R is much greater in the 5 mm shunt model as compared to the 4 mm shunt model, which is illustrated in the RFP in Figure 5.8(a) and Figure 5.8(b). Separation of flow exists for nearly 2.5 diameters distal to the throat in the 5 mm shunt, while only a small region of flow separation of approximately 0.5 diameters is observed in the 4 mm shunt (Figure 5.11). Velocity profiles just downstream of the constriction also show reverse flow during most of the oscillatory cycle for a 5 mm shunt (Figure 5.9).

Figure 5.12 shows the average shear rate along the top wall distal to the throat for both a 4 mm and 5 mm shunt. Although earlier results indicated similar maximum shear stresses during peak systole in both models, it can be seen that the average shear rate along the top wall is almost three times greater in the 5 mm shunt. The shear rate waveforms seen in the two shunts downstream of the constriction show the consistency of the pump over complete pulse cycles (Figure 5.13). The skin friction coefficient (C_f), based upon a previously determined characteristic velocity, along the top wall downstream of the constriction at various phases of the pulsatile cycle is illustrated in Figure 5.14. This shows the maximum value of C_f is almost twice as high in the 5 mm shunt.

Preliminary data has also been collected from an arterial tree flow circuit, which includes a correctly dimensioned aortic arch and realistic vessel angles. This closed-loop system, with entrance and exit effects, should better approximate flow characteristics through an adjustable SPA shunt. Figure 5.15 shows the velocity vectors at the inlet of a 4 mm shunt under steady flow conditions. The inlet flow is not uniform across the shunt due to entrance effects. Figure 5.16 shows that recirculation areas are still visible distal to the throat, although reattachment length is much shorter possibly due to entrance effects. Flow reattaches and is uniform at the shunt exit.

	Asymmetric Constriction		Axisymmetric Constriction	
Steady Flow	V_{MAX}	16.7 cm/s±1.6 cm/s	V_{MAX}	13.5 cm/s±1.1 cm/s
	$Vorticity_{MAX}$	66.2 /s ± 6.3 /s	$Vorticity_{MAX}$	48.9 /s ± 4.2 /s
	L_R	2.5 D	L_R	0 D
Pulsatile Flow	V_{MAX}	14.2 cm/s±2.5 cm/s	V_{MAX}	13.4 cm/s±1.8 cm/s
	$Vorticity_{MAX}$	52.7 /s ±11.7 /s	$Vorticity_{MAX}$	43.3 /s ± 8.5 /s
	L_R	0.5 D	L_R	0 D

Table 5.1: Results for asymmetric and axisymmetric constriction of a 4 mm shunt under steady and pulsatile flow. The axisymmetric constriction was formed by matching the cross-sectional area through the throat of an asymmetric constriction.

	Asymmetric Constriction		Axisymmetric Constriction	
Steady Flow	V_{MAX}	32.4 cm/s±7.7 cm/s	V_{MAX}	25.0 cm/s±2.4 cm/s
	$Vorticity_{MAX}$	135.4 /s ± 34.1 /s	$Vorticity_{MAX}$	92.1 /s ± 8.2 /s
	L_R	2.0 D	L_R	1.0 D
Pulsatile Flow	V_{MAX}	23.5 cm/s±4.5 cm/s	V_{MAX}	21.6 cm/s±3.0 cm/s
	$Vorticity_{MAX}$	78.8 /s ± 19.0 /s	$Vorticity_{MAX}$	77.5 /s ± 14.1 /s
	L_R	2.0 D	L_R	1.25 D

Table 5.2: Results for asymmetric and axisymmetric constriction of a 5 mm shunt under steady and pulsatile flow. The axisymmetric constriction was formed by matching the cross-sectional area through the throat of an asymmetric constriction.

4 mm Shunt		
Quantity	0-2 D downstream	2-4 D downstream
V_{MAX}	29.04 cm/s ± 3.0 cm/s	26.08 cm/s ± 2.5 cm/s
$Vorticity_{MAX}$	175.2 /s ± 17.7 /s	162.7 /s ± 16.4 /s
5 mm Shunt		
Quantity	0-2 D downstream	2-4 D downstream
V_{MAX}	35.04 cm/s ± 3.9 cm/s	25.25 cm/s ± 3.1 cm/s
$Vorticity_{MAX}$	255.7 /s ± 32.0 /s	156.3 /s ± 24.7 /s

Table 5.3: Maximum values of velocity and vorticity downstream of the constriction in a 4 mm and 5 mm shunt.

Shunt Size (mm)	Shear Rate (s^{-1})	Shear Stress (dynes/cm^2)
3.5	212.1	6.8
4.0	606.8	19.4
5.0	641.6	20.5

Table 5.4: Maximum values of shear rate and shear stress during systole in a 3.5 mm, 4.0 mm, 5.0 mm shunt

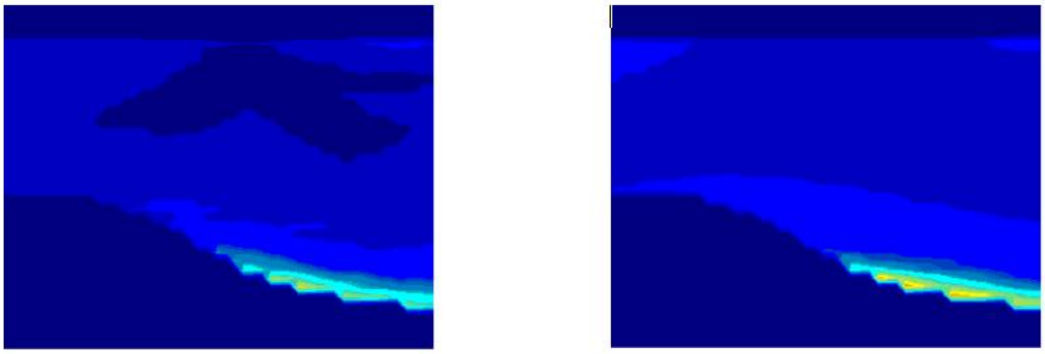

Figure 5.1: Example of RFP in a 4 mm flow model for two independent test samples. Similarity between images demonstrates reproducability and validates experimental results.

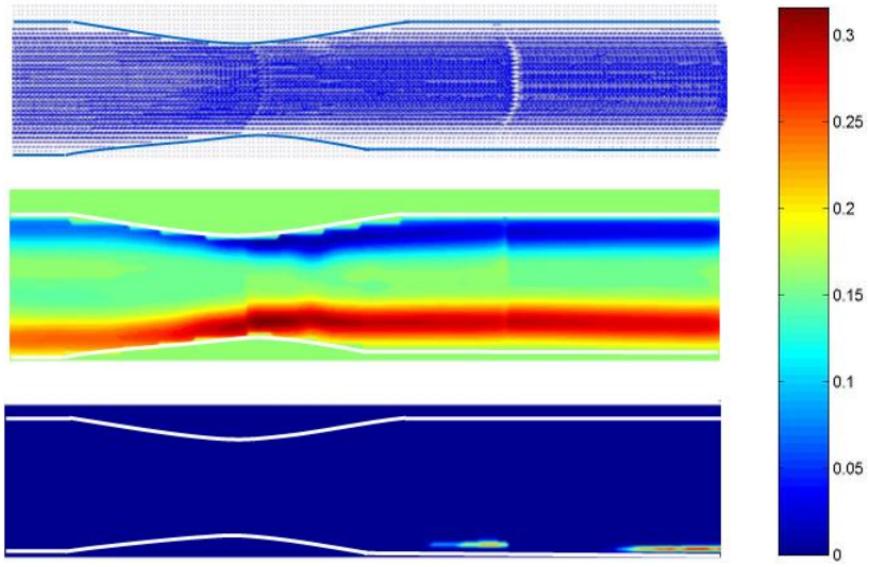

(a)

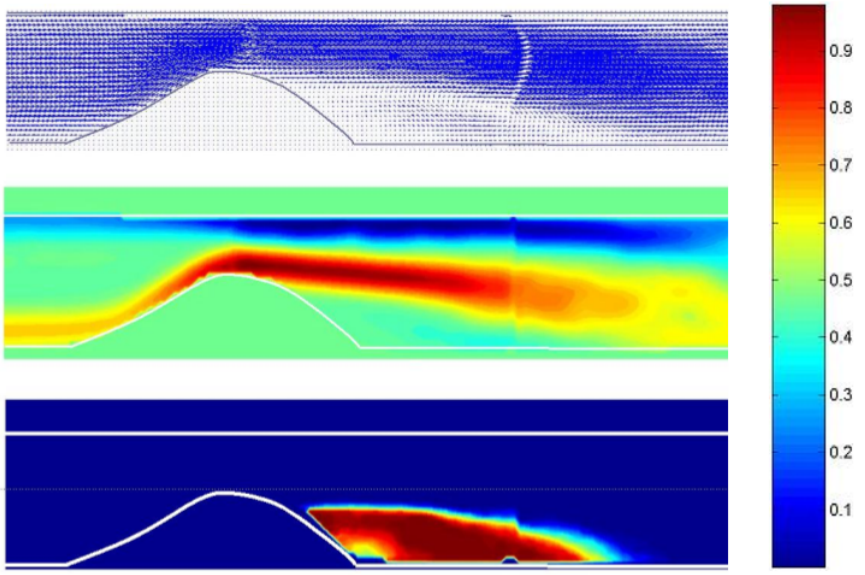

(b)

Figure 5.2: Average velocity vectors (top), vorticity (middle), and RFP (bottom) shown for steady flow through an axisymmetric and asymmetric 4 mm shunt with a *Re* of 1061.

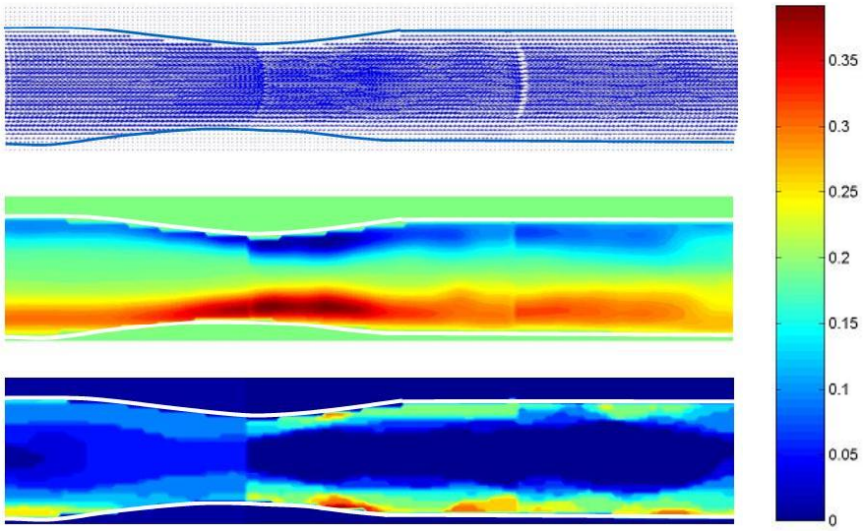

(a)

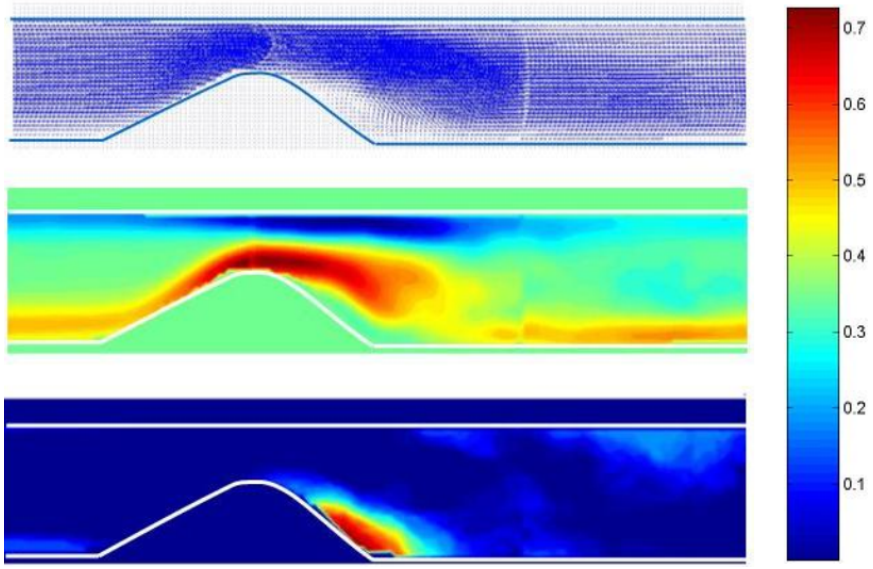

(b)

Figure 5.3: Average velocity vectors (top), vorticity (middle), and RFP (bottom) shown for a complete cycle of pulsatile flow through an axisymmetric and asymmetric 4 mm shunt with a Re of 1061 and α of 23.14

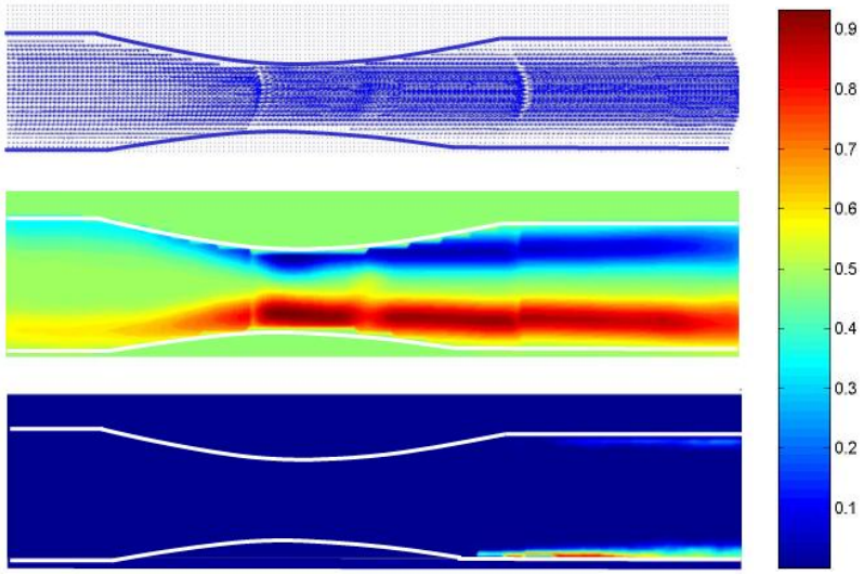

(a)

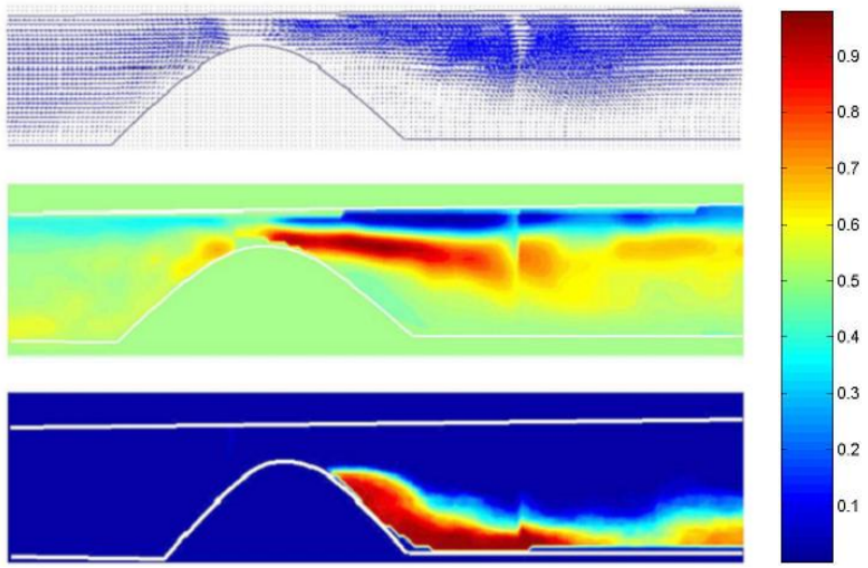

(b)

Figure 5.4: Average velocity vectors (top), vorticity (middle), and RFP (bottom) shown for steady flow through an axisymmetric and asymmetric 5 mm shunt with a *Re* of 1061.

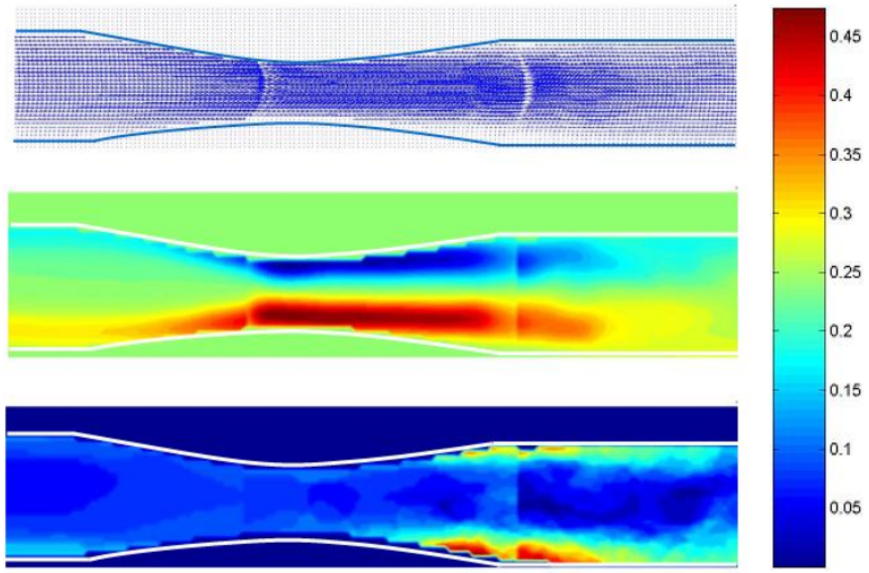

(a)

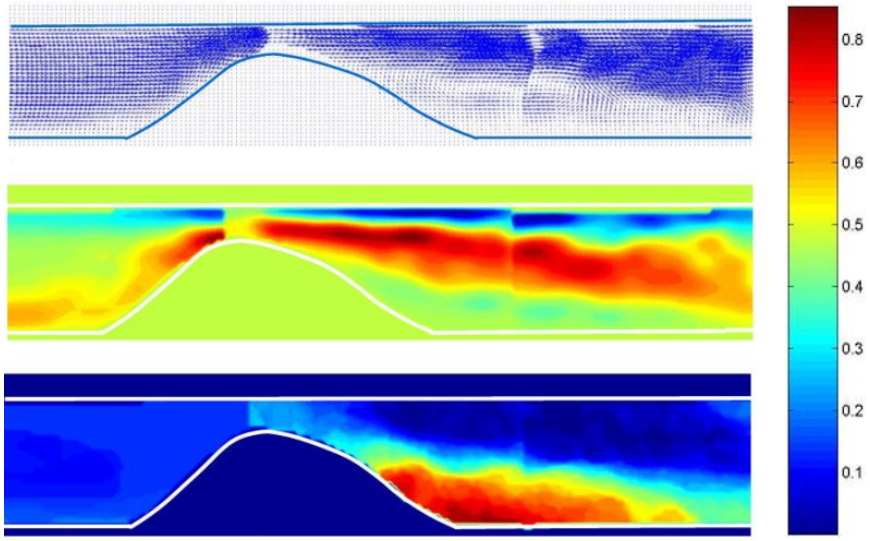

(b)

Figure 5.5: Average velocity vectors (top), vorticity (middle), and RFP (bottom) shown for a complete cycle of pulsatile flow through an axisymmetric and asymmetric 5 mm shunt with a Re of 1061 and α of 23.14

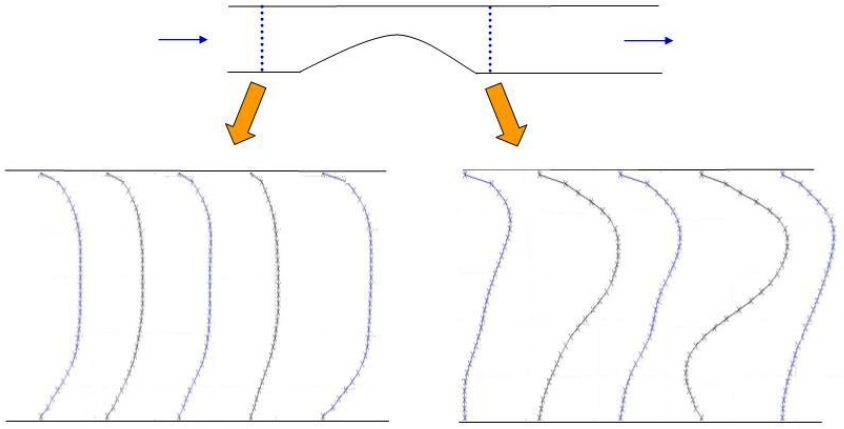

(a)

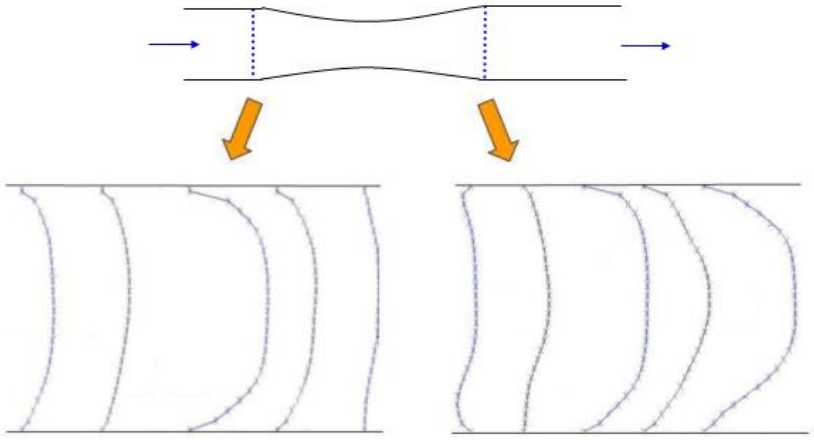

(b)

Figure 5.6: Velocity profiles for 1 pulsatile cycle at two different locations in a 4 mm constricted shunt. Time interval between profiles is $t \approx 0.1s$

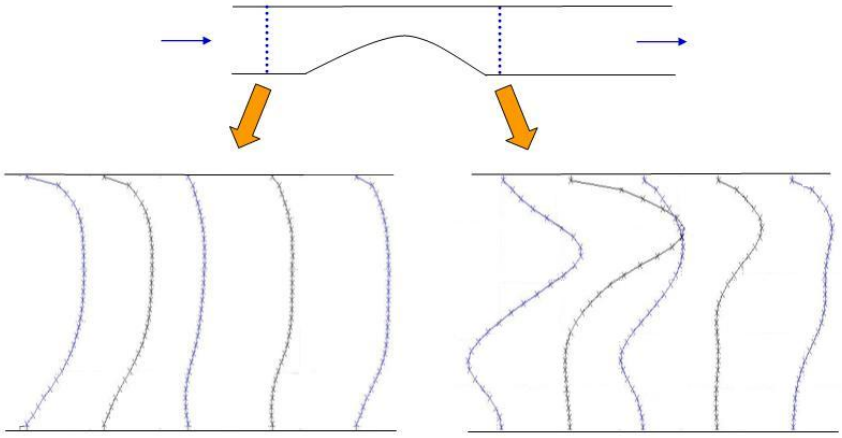

(a)

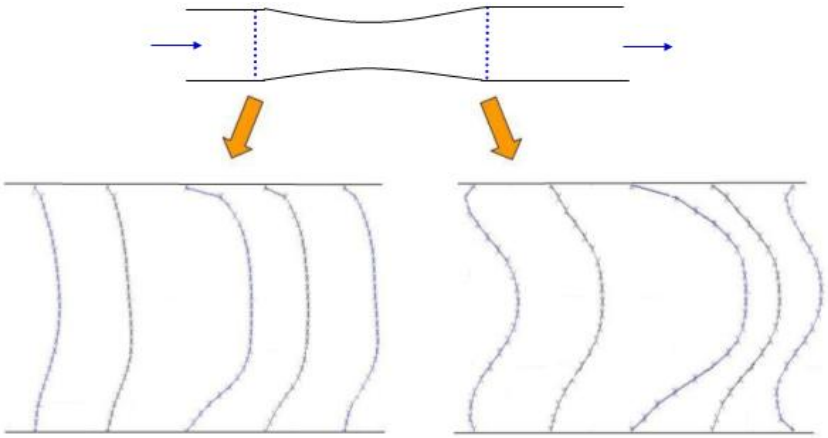

(b)

Figure 5.7: Velocity profiles for 1 pulsatile cycle at two different locations in a 5 mm constricted shunt. Time interval between profiles is $t \approx 0.1s$

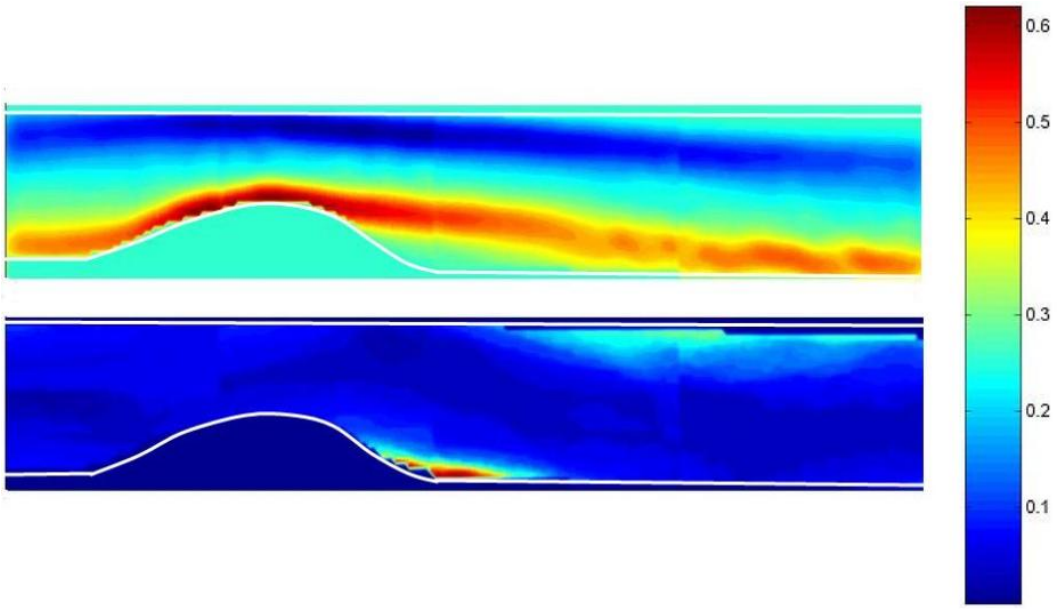

(a)

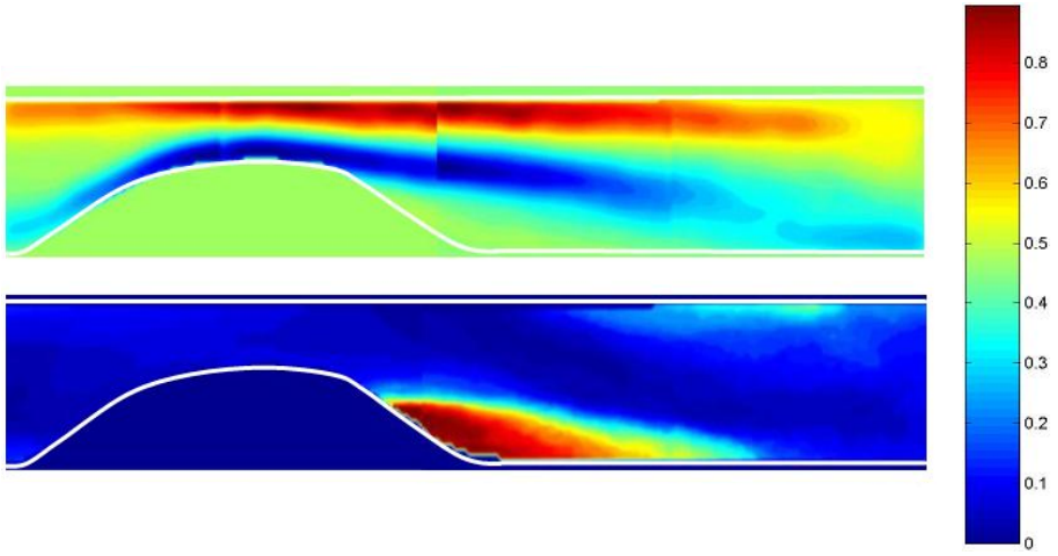

(b)

Figure 5.8: Average vorticity and RFP shown for a complete cycle of pulsatile flow through (a) a constricted 4 mm shunt matching Re of 1061 and α of 4.09, and (b) a constricted 5 mm shunt matching Re of 849 and α 5.12 as seen *in vivo*.

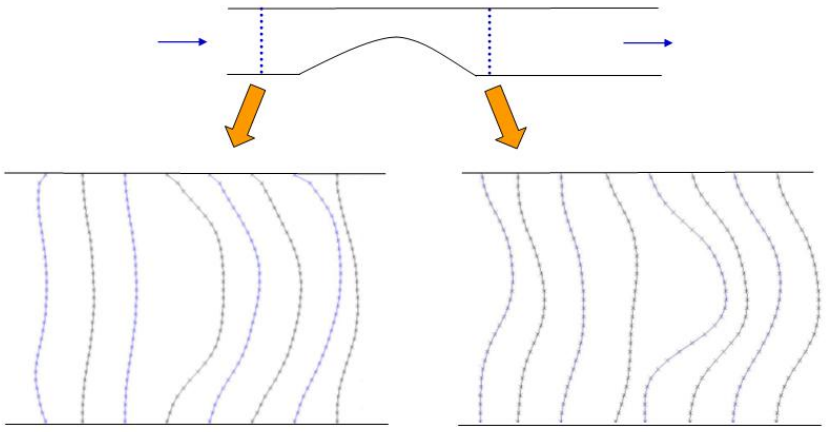

(a)

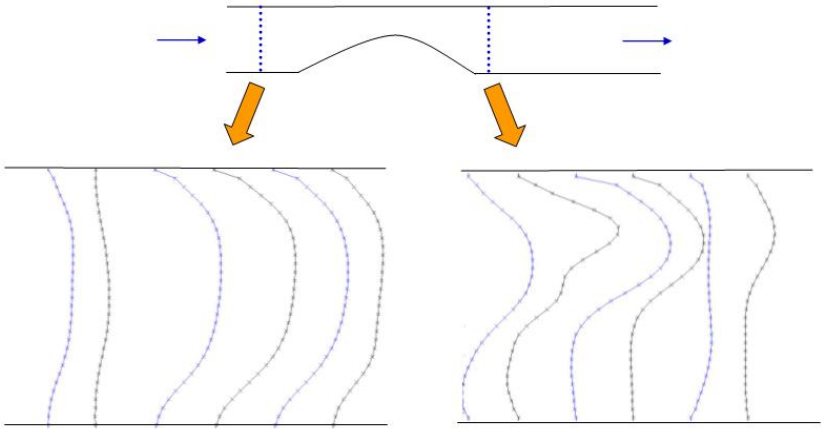

(b)

Figure 5.9: Velocity profiles for 1 pulsatile cycle proximal and distal to the constriction in a 4 mm shunt (a) with a Re and α of 1061 and 4.09 respectively, and a 5 mm shunt (b) with a Re and α of 849 and 5.12. Time interval between profiles is $t \approx 0.42s$ for the 4 mm shunt and $t \approx 0.42s$ for the 5 mm shunt.

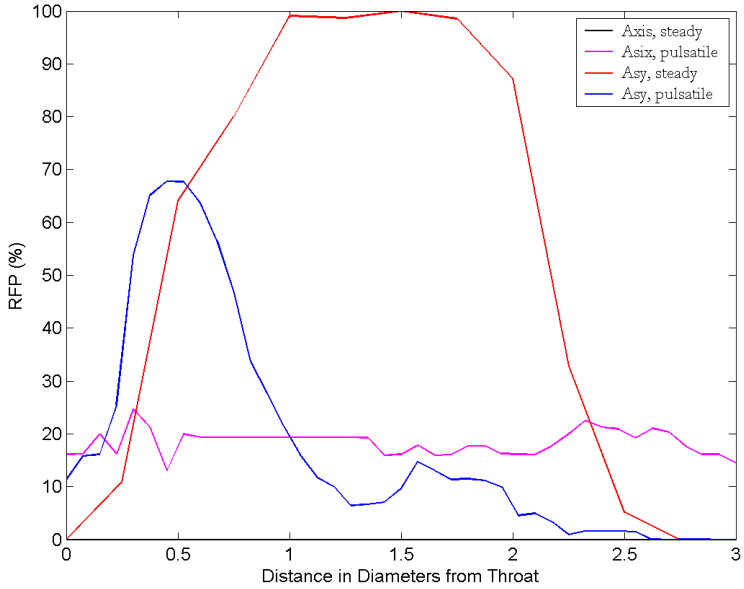

(a)

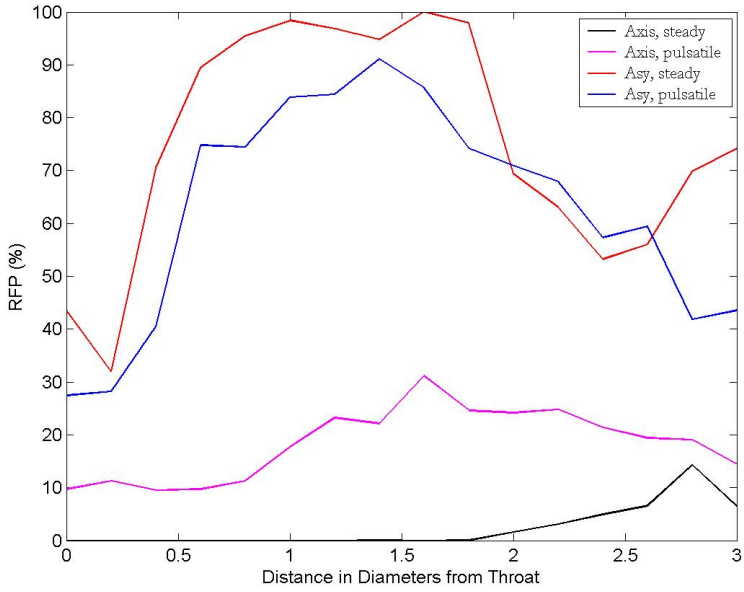

(b)

Figure 5.10: Average probability of reverse flow in both an axisymmetric and asymmetric constriction in (a) 4 mm and (b) 5 mm shunts under steady and pulsatile conditions.

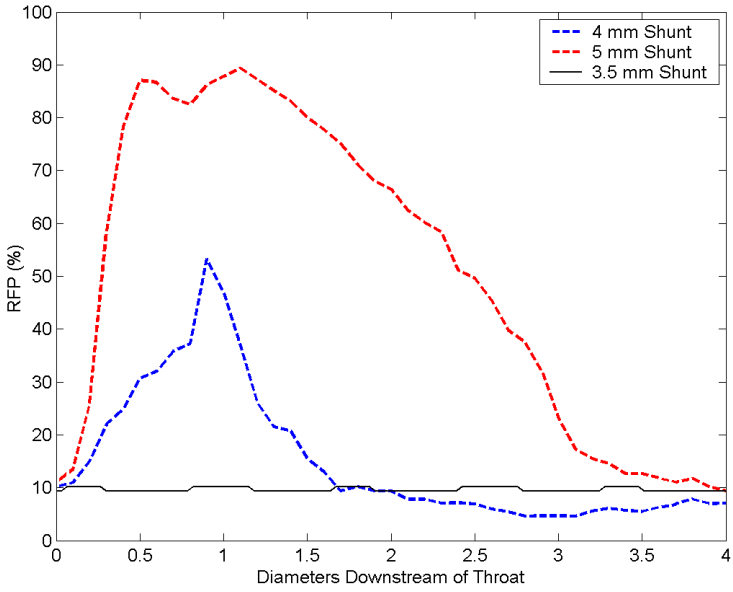

Figure 5.11: Average probability of reverse flow in a 4 mm shunt matching Re of 1061 and α of 4.09, and a 5 mm shunt matching Re of 849 and α of 5.12 as seen *in vivo*.

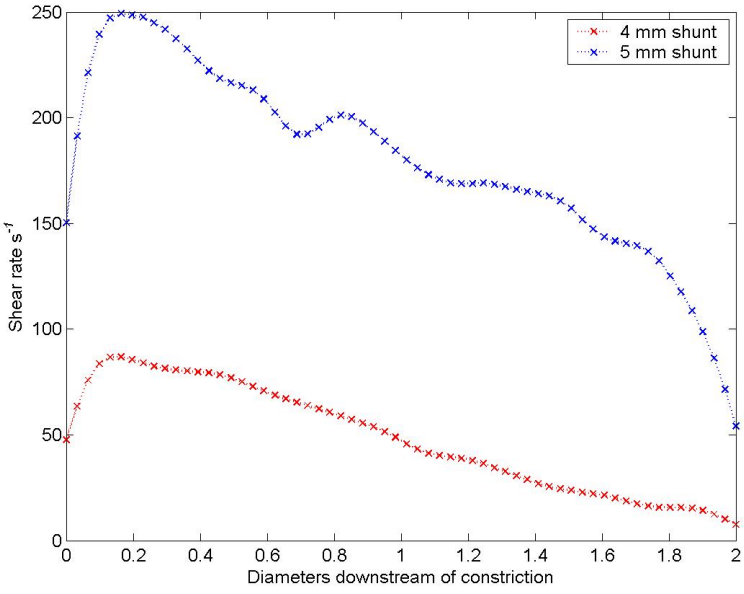

Figure 5.12: Mean shear rate along the top wall for both 4 mm and 5 mm asymmetrically constricted shunts from 0-2 diameters distal to the throat.

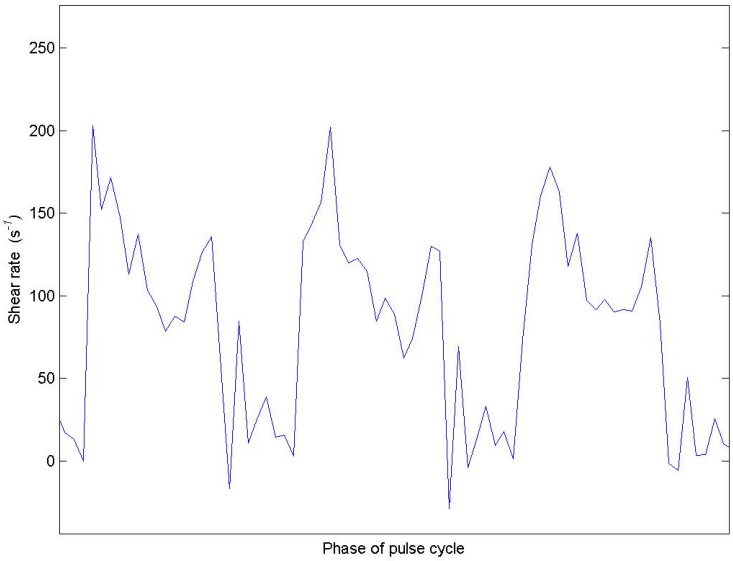

(a)

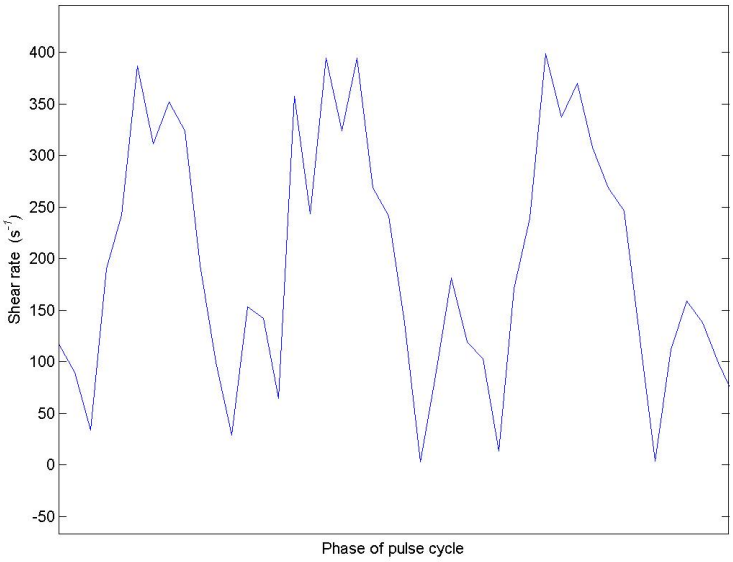

(b)

Figure 5.13: Shear rate waveforms for 3 periods of pulsatile flow distal to the throat in (a) a 4 mm shunt matching Re of 1061 and α of 4.09, and (b) a 5 mm shunt matching Re of 849 and α of 5.12 as seen *in vivo*.

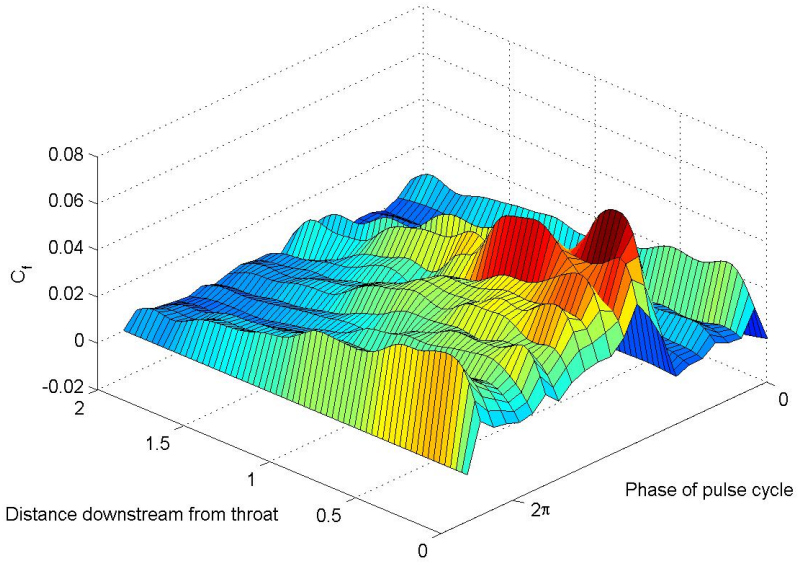

(a)

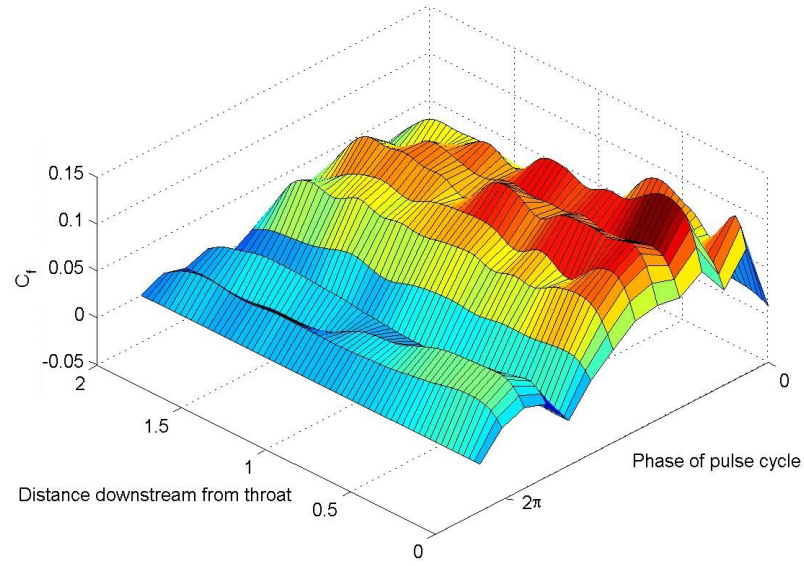

(b)

Figure 5.14: Skin friction coefficient along the top wall of (a) a 4 mm shunt and (b) a 5 mm shunt distal to the throat over one complete pulse cycle.

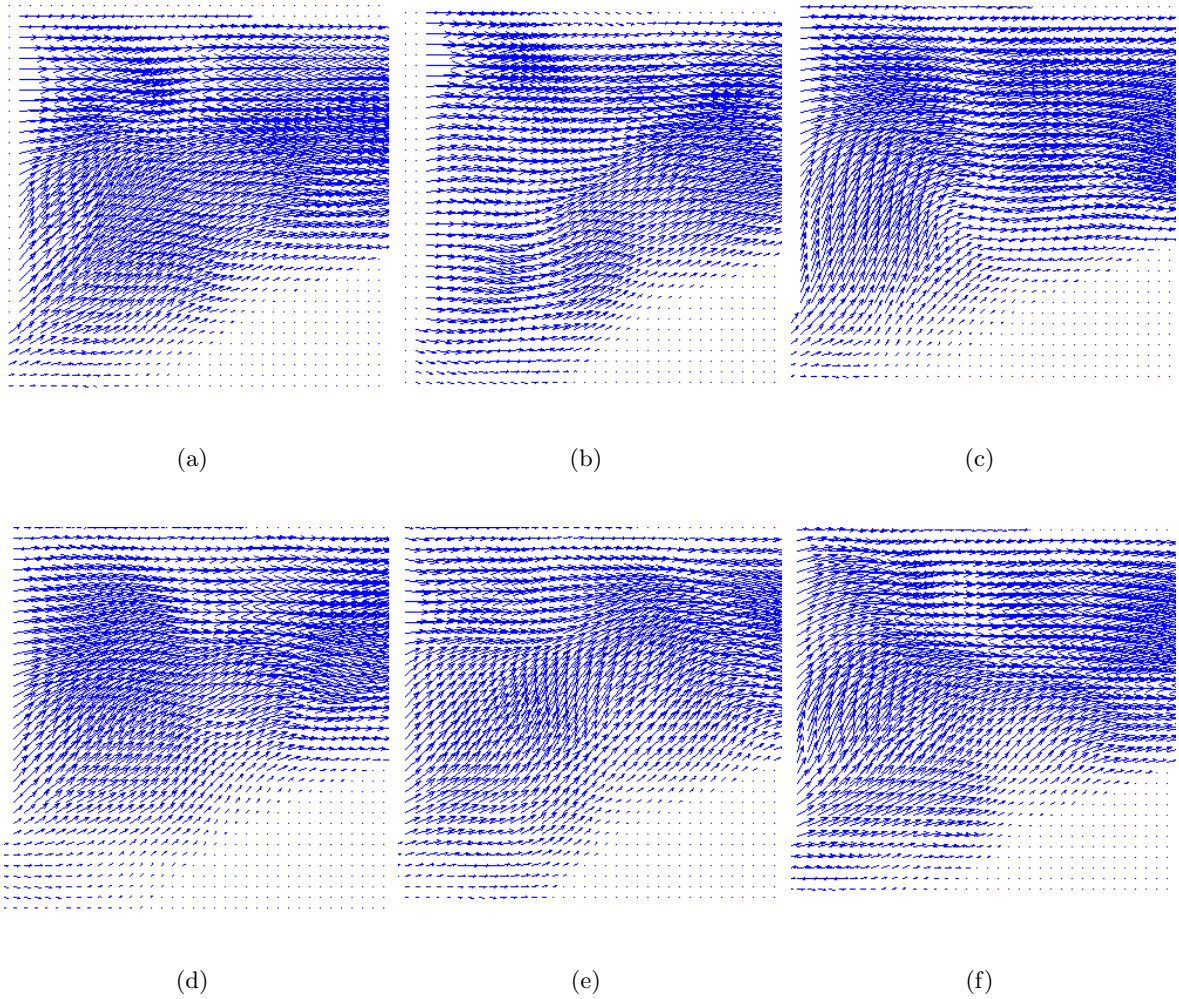

(a) (b) (c)

(d) (e) (f)

Figure 5.15: Velocity vectors at the entrance of a 4 mm shunt under steady flow conditions in the arterial tree flow circuit. Entrance effects alter steady flow at specific points in time.

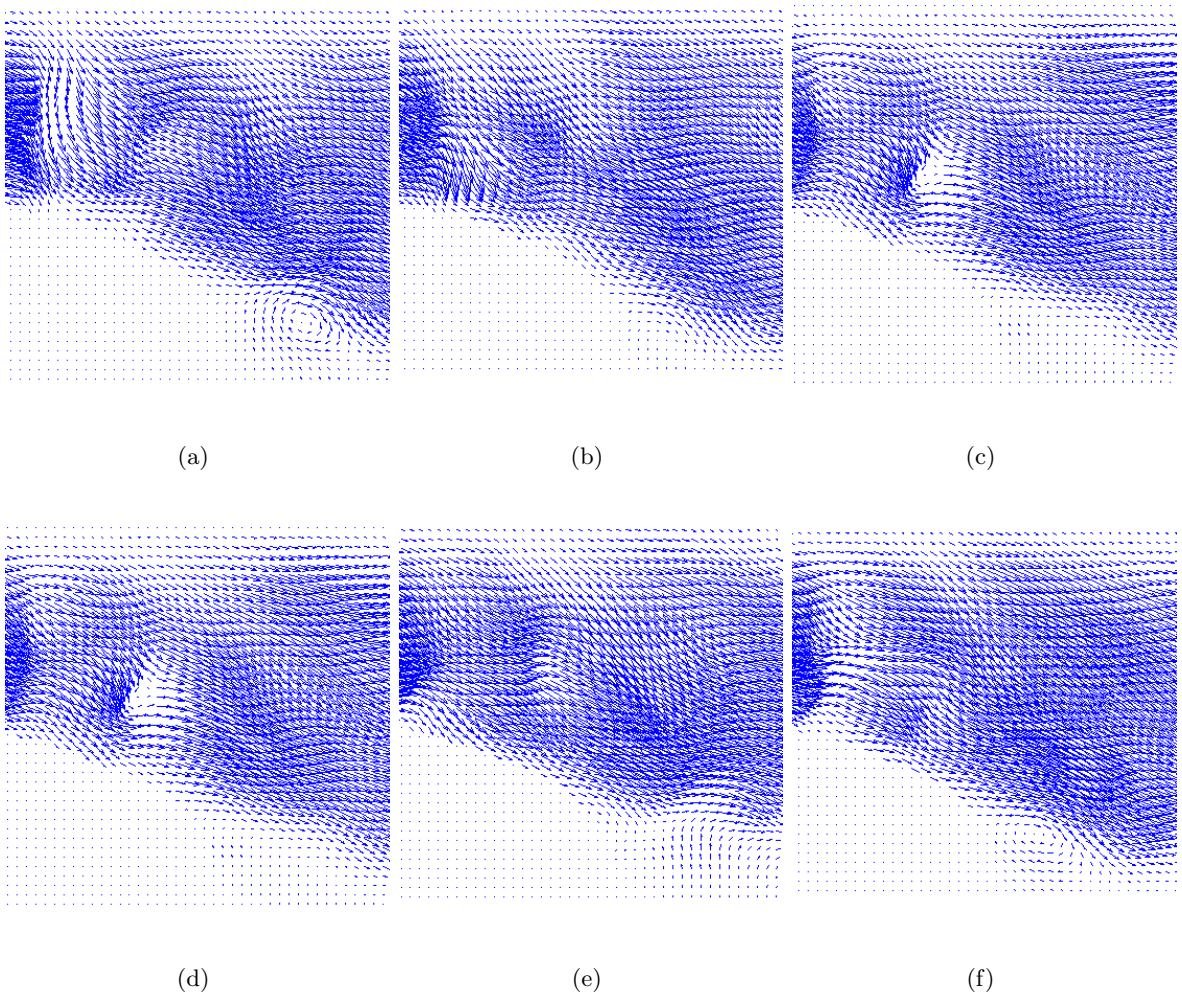

(a) (b) (c)

(d) (e) (f)

Figure 5.16: Velocity vectors distal to the constriction in a 4 mm shunt under steady flow conditions in the arterial tree flow circuit. Reattachment length decreases due to entrance effects.

Chapter 6

Discussion

The first part of this study involved creating a mock flow circuit of an infant's arterial circulatory system used to verify the flow rate through an open 3.5 mm shunt matching *in vivo* parameters. The flow rate was determined to be approximately 600 cc/min. This average flow rate agrees with Doppler measurements recorded at the proximal and distal portions of a 3.5 mm shunt in two patients following first-stage Norwood operations [30]. Therefore, the average flow rates and the level of constrictions in the adjustable 4 mm and 5 mm shunts are the same as what would be seen *in vivo*.

6.1 Asymmetric vs. Axisymmetric

One of the goals of this study was to determine the effects on the flow fields of an adjustable SPA shunt with two different forms of constriction. Although the results obtained from the tests in this part of the overall study are not applicable to the situation *in vivo* (Womersley number was not matched), they are still useful in establishing the relative differences in flow fields between the two constrictions. Comparing between pulsatile and steady flow, both the asymmetric and axisymmetric constrictions demonstrated lower values of maximum velocity and vorticity for pulsatile flow. This observation can be explained by the fact that at high frequency, oscillatory flow in a tube does not have enough time to reach a fully developed Poiseuille flow profile, which is seen in the steady flow case. The oscillatory velocity profiles before the constriction in the tube exhibit blunted curves rather than the parabolic shapes observed during steady flow. These lower peak velocities observed for pulsatile flow as compared with steady flow are most likely due to the higher Womersley Number (α) [17].

The results also show that differences in the maximum average velocity and vorticity between

an ideal axisymmetric and the actual asymmetric constriction do exist under both flow conditions, although these differences are magnified in a 5 mm shunt. This observation would seem to indicate that the greater the reduction in flow, the greater the influence the type of constriction has upon the flow fields. In other words, a severely constricted shunt will demonstrate significantly lower maximum values of velocity and shear rate in an axisymmetric constriction as opposed to an asymmetric constriction for the same inlet flow.

The main difference between the two constrictions, though, is seen in the RFP. Flow separation is much greater in an asymmetric constriction, where there is a bigger adverse pressure gradient downstream of the constriction. In pulsatile flow, these regions of flow separation occur only during the systolic cycle where particle velocity is a maximum. During the diastolic cycle of the oscillatory flow (when the pump or heart is refilling), flow is able to reattach, as shown by the velocity profiles Figures 5.6 and 5.7. Figure 5.10(a) clearly illustrates the increased probability of reversed flow between the two constrictions. For an axisymmetric 4 mm shunt, probability of reverse flow is zero under steady flow conditions and for pulsatile flow remains constant at approximately 20%. This is expected for oscillatory flow since flow slows downs and begins to recirculate at the walls just prior to the systolic cycle. However, for the asymmetric 4 mm shunt under pulsatile flow, RFP is around 70% immediately distal to the constriction. Since regions of low flow *in vivo* are known to provide areas of plaque depostion [**?**], this increase in reverse flow could lead to greater plaque deposition in the asymmetric constriction. Similar results are seen in Figure 5.10(b) for the 5 mm model. The increase in RFP for steady flow through the axisymmetric 5 mm model seen 2-3 diameters downstream of the constriction is most likely due to the presence of bubbles in the water-filled optical box. These bubbles give a false indication of flow reversal along the bottom of the axisymmetric models, which can also be seen in Figure 5.2(a) and Figure 5.4(a). For the asymmetric constriction, RFP above 40% is observed for steady and pulsatile flow throughout the length of the collected area. Since data was only collected approximately 3 diameters downstream of the throat, it is difficult to tell exactly when flow completely reattaches in the 5 mm shunt.

One of the problems with the glass models used in this study is the accuracy in flow reduction between the asymmetric and axisymmetric constriction. Since a prototype of the initial design using an ideal axisymmetric constriction was never created, models of axisymmetric constrictions were paired with their asymmetric counterparts by roughly matching the cross-sectional area through the throat. This leads to two problems: (1) a greater decrease in cross-sectional area may be required with an axisymmetric constriction to equal the same flow reduction achieved with an asymmetric constriction, and (2) it is difficult to get an accurate matchup of the two constrictions

based upon the cross-sectional area. Still, this study demonstrates the major differences in the flow fields between the two constrictions, which should be taken into consideration if future design modifications to the adjustable SPA shunt are necessary.

6.2 Matching Dimensionless Parameters

For the tests in which both *Re* and α were matched, the shear rates observed in the models are theoretically the values that would be observed *in vivo*. Maximum shear rates in both a 4 mm and a 5 mm constricted shunt were found to be approximately 607 s^{-1} and 642 s^{-1}, respectively. These maximum values occur during systole, and are more than 3 times the shear rate seen in the open 3.5 mm shunt 5.4. However, these values are well under the minimum shear stress previously shown to induce platelet aggregation [4]. Although the differences in the maximum shear rates between the 4 mm and 5 mm shunt initially seem minimal, a closer inspection near the top walls of the models shows that the average shear rate (not maximum) distal to the throat is nearly 3 times greater in a 5 mm shunt. C_f is also shown to be twice as great during peak systole in a 5 mm shunt. Therefore, although the maximum shear rates are almost equal, average shear rates distal to the throat along the shunt walls are much higher in a 5 mm shunt. Still, it would appear that an adjustable systemic-pulmonary artery shunt as designed for this study does not generate the required levels of shear stress to produce blood cell damage. The safety factor is approximately 5.

Another important difference observed between the two models is the length of flow separation. For the 4 mm shunt, L_R occurs 0.5 diameters downstream of the throat. The beginning of vortices forming during systole can also be seen along the top wall 1-2 diameters downstream. For a 5 mm shunt, a much larger area of recirculation is observed, with a L_R of 2.5 diameters distal to the throat. Figure 5.11 shows that for a 3.5 mm shunt, RFP is around 10%, which occurs at the end of the diastolic cycle. This region of low flow in the 4 mm and 5 mm models increases the risk of plaque formation and platelet aggregation, a clinical concern since this could lead to thromboses. RFP of around 35% is also present along the top wall 2-3 diameters downstream.

One of the assumptions made in the PIV circuit is that flow is fully developed. Yet the entry length required for fully developed flow is much greater than the length of an SPA shunt (see Chapter 3). Preliminary data from the arterial tree flow circuit indicates that under steady flow conditions entrance and exit effects do influence the flow characteristics downstream of the constriction. Further investigation is needed to determine the affects, if any, of partially developed pulsatile flow and wave reflections on vorticity and flow reversal.

Chapter 7

Summary

7.1 Conclusions

This study effectively demonstrates the changes in flow fields through an adjustable systemic-pulmonary artery shunt using PIV. The maximum value of shear stress observed in an actual 4mm and 5 mm adjustable SPA shunt are 19.4 dynes/cm^2 and 20.5 dynes/cm^2, respectively. This is well within an allowable shear stress range of 100 dynes/cm^2 without leading to platelet aggregation. However, a concern with an adjustable SPA shunt is the possibility of plaque build-up in areas of low flow immediately following the constriction. The PIV results indicate that for the same flow rates, smaller areas of flow reversal would be expected for a 4 mm constricted shunt as compared to a 5 mm constricted shunt. Although the shunt will only be in place for 6 months, it is difficult to predict from the data the effect this will have upon plaque formation. *In vivo* testing will likely be needed to assess the risk of thrombosis. Flow reversal distal to the throat was shown to be much greater in an asymmetric constriction as opposed to the ideal axisymmetric constriction. Therefore, if it is determined that an asymmetric constriction presents to large of a clinical risk, then a new mechanism forming an axisymmetric constriction should be considered.

7.2 Future Work

Further *in vitro* testing should include additional PIV experiments using the PIV flow system that mimicks an infant's arterial tree. This system, with entrance and exit effects, will more realistically match flow through a shunt. Future work also should include a computational study of steady and pulsatile flow using the geometrically accurate 3-D CAD models, as well as an *in vivo* study in animals addressing the concern of plaque formation. Continual work is being performed

on the design of the graft/resistor mechanism and the controller unit.

Appendix A

The Effect of Pulse Pressure on Shunt Flow

A.1 Objective

Physiological or pharmacological manipulations which increase systemic vascular resistance (SVR) and/or lower pulmonary vascular resistance (PVR) are known to increase flow through an SPA shunt. Conversely, manipulations which increase PVR and lower SVR are thought to decrease SPA shunt flow. However, the impact of pulse pressure, with a constant mean blood pressure, is unknown. The purpose of this experiment was to determine the effects of pulse pressure on flow through an SPA shunt.

A.2 Materials and Methods

The *in vitro* flow circuit used to mimic single ventricle circulation is the same as the one described in Chapter 4 (Figure 4.1). The only difference from the setup described in those previous sections is the use of a Harvard Instruments pulsatile hydraulic pump. The parameters on the pulsatile pump were set to match the frequency of an infants average heartbeat and stroke volume. Since an actual 4 mm shunt was used, both Re and a were matched as seen *in vivo*. The pulsatile waveforms generated by the hydraulic pump approximate that of a normal arterial pressure waveform (Figure A.1).

The shunt used in the experiment was a 4.0 mm PTFE vascular graft. The resistor mechanism used to vary shunt flow is described in Chapter 2 (Figure 2.4). For each trial, the pulsatile pump was set to a heart rate of 120 beats/minute and a stroke volume of 10 cc. Four different pulse-

pressures were utilized: 15, 25, 30, and 35 mmHg. Three different mean inlet (arterial) pressures were utilized: 40, 50, and 60 mmHg. These inlet pressures correspond to the range commonly seen in neonates following cardiac surgery. The various pulse-pressures were achieved by altering the compliance of the latex tubing in the system and adjusting the screw clamps. The initial outlet (pulmonary) pressure was set to 20 mmHg by adjusting the pulmonary vascular resistance (PVR) screw clamp when the when the inlet pressure was 40 mmHg. The PVR was then left unaltered for the remainder of the trials at that pulse pressure. The flow through the shunt was then measured with the set inlet pressure at each of the four pulse pressures. This was then repeated at inlet pressures of 50 and 60 mmHg. The total number of trials was 15 per pulse pressure. All data was acquired using Labview (National Instruments) program Biobench. Data was statistically analyzed with the Statistical Analysis System (SAS) program using a 2 factor ANOVA test.

A.3 Results

A bar graph plotting shunt flow (cc/min) versus mean inlet pressure (mmHg) is shown in Figure A.3.1. This analysis demonstrates that the change in shunt flow, while varying the pulse pressures within a given inlet pressure, was not statistically significant for each combination. Perhaps even more importantly, there was no trend towards clinical significance with the greatest percentage difference between two different pulse pressures (15 vs. 30 mm pulse pressure with an inlet pressure of 50 mmHg) only 3.5

A.4 Conclusions

The data demonstrates that flow through the shunt increases with increasing inlet pressures as would be expected. However, flow is not affected by changing the pulse pressure for the same mean inlet and outlet pressure.

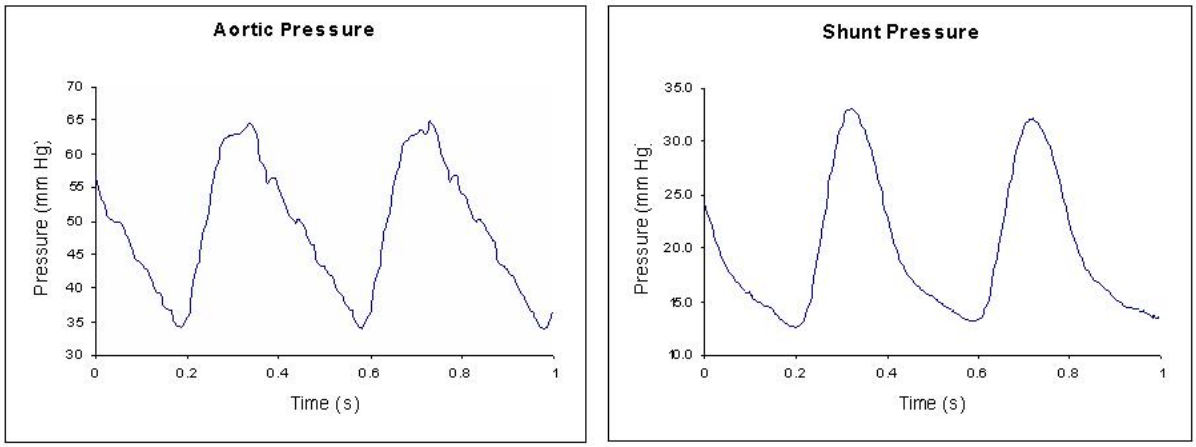

Figure A.1: Pressure waveforms generated by the hydraulic pump.

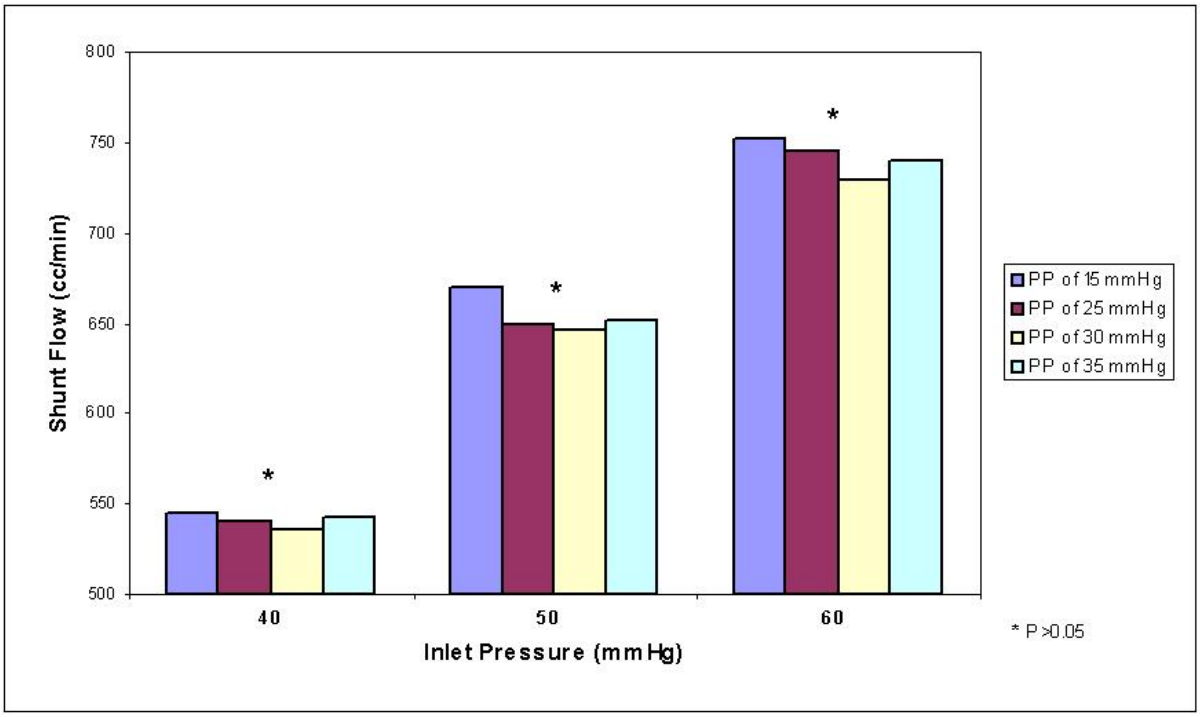

Figure A.2: Shunt flow at varying mean inlet and pulse pressures.

Appendix B

QuantIm Scripts

The following QuantIm scripts were used for image acquisition and processing of the cross-sections of the sliced shunts. The first script was needed for calibration to determine the number of pixels/cm in the series of images. The second script was used to capture an image after each cross-sectional slice. Since the cutting blade on which the camera was mounted did not return to the exact position after each slice, the third script was needed to align all the images to the center of a fiducial mark. The fourth script was used to output a file containing (x,y) coordinates of the lumen outline for each image.

B.1 Calibration of Image Size

```
Run
Load_LUT "C:\QuantIm\LUTs\gray.lut"
Read_Variable "Enter number of images" "num_images"
Open "C:\Tim\Quantim\Images\Shunt4.0@3.5\calibration*.tif" A 1 !num_images 1 10
Math !num_images "-" 0.000000 "last_image"
Select_Image A 1 !last_image
Set_Images B !num_images 640 480 8 "PC"
Calibrate A 1 1.000000 1.000000 T T "mm" 2.000000 2.000000
Set_Variable "i" 1.000000
Label "LoopTop"
High_Pass A !i B 1 97 97 F 128
Display B 1
Segment B 1 B 2 T T 0 255 0 255 0 255 "And"
Set_Draw_Mode F "COPY" 0 0 2 F "*times*24*" 255 255 255 F
Draw_Free B 2 F
Set_Draw_Mode F "COPY" 255 255 2 F "*times*24*" 255 255 255 F
Draw_Free B 2 F
Set_Images C !num_images 640 480 16 "PC"
Identify B 2 C 0 A 3 "Full_image" T
Run
```

```
Display C 0
Scrap C 0 C 1 400
Display C 1
Select_Objects C 1 C 2 T F "Area" 1.000000 100.000000
Display C 2
Convert_Ident C 2 C 3 F
Copy_Image C 3 B 3
Display B 3
Autofill B 3 B 4 0
Display B 4
Identify B 4 B 6 B 6 "Full_image" T
Display B 6
Convert_Ident B 6 B 8 F
Ranking B 8 B 9 7 7 25
Display B 9
Identify B 9 B 10 B 9 "Full_image" T
Display B 10
Contour B 10 B 11 4
Display B 11
Copy_Image B 11 A !i
Display A !i
Pause
Object_to_ASCII A !i 1 "C:\Tim\Quantim\Images\Shunt35-2\Shunt_3"
Run
Loop "LoopTop" "i" !num_images
Pause
```

B.2 Image Acquisition

```
Run
Load_LUT "C:\QuantIm\LUTs\gray.lut"
Set_Images A 40 640 480 8 "PC"
Meteor_Setup "RCA" "NTSC" F F F
Meteor_Live A 0
Pause
Save "C:\Tim\Quantim\Images\Shunt4.0@75%3.5\tim35.tif" A 0 1 "TIFF-P"
Pause
```

B.3 Image Alignment

```
Run
Load_LUT "C:\QuantIm\LUTs\gray.lut"
Read_Variable "Enter number of images" "num_images"
Open "C:\Tim\Quantim\Images\Shunt35-2\tim*.tif" A 0 !num_images 1 0
Math !num_images "-" 1.000000 "last_image"
Select_Image A 0 !last_image
Set_Images B 10 640 480 8 "PC"
Set_Images C 10 640 480 16 "PC"
Calibrate C 1 1.000000 1.000000 F T "Pixel" 1.000000 1.000000
```

```
Run
Set_Variable "i" 0.000000
High_Pass A !i B 0 97 97 F 128
Display B 0
Segment B 0 B 1 T T 0 255 0 255 0 255 "And"
Display B 1
Ranking B 1 B 2 5 5 13
Display B 2
Identify B 2 B 3 B 1 "Full_image" T
Display B 3
Select_Objects B 3 B 4 T F "Area" 1.000000 100.000000
Autofill B 4 B 5 0
Display B 5
Identify B 5 B 6 B 6 "Full_image" T
Measure B 6 B 0 F
Data_to_Variable "ref_x0" 1 "Center X"
Data_to_Variable "ref_y0" 1 "Center Y"
Math !ref_x0 "-" 100.000000 "ref_x1"
Set_Variable "ref_y1" !ref_y0
Set_Variable "i" 1.000000
Label "LoopTop"
High_Pass A !i B 0 97 97 F 128
Window B 0 F 0 255
Display B 0
Segment B 0 B 1 T T 0 255 0 255 0 255 "And"
Ranking B 1 B 2 5 5 13
Display B 2
Identify B 2 B 3 B 3 "Full_image" T
Select_Objects B 3 B 4 T F "Area" 1.000000 100.000000
Autofill B 4 B 5 0
Identify B 5 B 6 B 6 "Full_image" T
Measure B 6 B 0 F
Data_to_Variable "x0" 1 "Center X"
Data_to_Variable "y0" 1 "Center Y"
Math !x0 "-" 100.000000 "x1"
Set_Variable "y1" !y0
Match_Images A 0 A !i B 7 F !ref_x0 !ref_y0 !ref_x1 !ref_y1 !x0 !y0 !x1 !y1
Display B 7
Window B 7 F 0 255
Copy_Image B 7 A !i
Display A !i
Loop "LoopTop" "i" !last_image
Select_Image A 0 !last_image
Pause
Save "C:\Tim\Quantim\Images\Shunt35-2\tim_Shift_*.tif" A 0 !num_images "TIFF-P"
Pause
```

B.4 Image Processing: Output of Lumen Coordinates

```
Run
```

```
Load_LUT "C:\QuantIm\LUTs\gray.lut"
Set_Images A 40 640 480 8 "PC"
Pause
Open "C:\Tim\Quantim\Images\tim_Shift_1.tif" A 0 1 1 0
Run
High_Pass A 0 A 1 97 97 F 128
Display A 1
Segment A 1 A 2 T T 0 255 0 255 0 255 "And"
Set_Draw_Mode F "COPY" 0 0 3 F "*times*24*" 255 255 255 F
Draw_Free A 2 F
Set_Draw_Mode F "COPY" 255 255 3 F "*times*24*" 255 255 255 F
Draw_Free A 2 F
Set_Images B 5 640 480 16 "PC"
Identify A 2 B 0 A 3 "Full_image" T
Run
Display B 0
Scrap B 0 B 1 400
Display B 1
Select_Objects B 1 B 2 T F "Area" 1.000000 100.000000
Display B 2
Convert_Ident B 2 B 3 F
Copy_Image B 3 A 3
Display A 3
Autofill A 3 A 4 0
Display A 4
Identify A 4 A 6 A 6 "Full_image" T
Display A 6
Convert_Ident A 6 A 8 F
Ranking A 8 A 9 7 7 25
Display A 9
Identify A 9 A 10 A 9 "Full_image" T
Display A 10
Contour A 10 A 11 4
Display A 11
Pause
Object_to_ASCII A 11 1 "C:\Tim\Quantim\Images\Shunt_*"
Pause
```

Appendix C

MATLAB Scripts and Input Files

C.1 MATLAB Scripts

The following MATLAB scripts were used for generating CAD models and in processing tensor files. The first script formatted the cross-section files created in QuantIm and generated a path line for solid modeling of the sections. The second script modified the raw mask generated with the XCap frame grabber in order to obtain 8-bit mask files to be used in WaLPT. The post-processing script reads the WaLPT output files (tensor files) and calculates maximum velocities and shear stresses and generates fields plots of vorticity, flow reversal, and skin friction. This file can be modified to further determine velocity profiles and plots of shear rate along the walls of the models. Also included is a sample WaLPT input file used to process the raw images [35]. This file can be modified to change window size and step size.

C.1.1 Formatting Cross-Sectional Geometry and Path Line Generation

```
interval=4;  %Decreases initial file size by incrementing between data points by  this interval value
gap = 0;
dist = 0;

disp('Number of Cross-section files to be converted:')
numb = input('');
disp('')


for i=0:numb-1;
    j=0;
    v=0;
    xcoor=0;
    ycoor=0;
    zcoor=0;
```

```
SectionX=0;
SectionY=0;

baseX=25;
baseY=0;
baseZ=0;
meanX=0;
meanY=0;

xmax=0;
xmin=1000;
ymax=0;
ymin=1000;

disp('ENTERING SECTIION')
disp('')

if i>0;
    disp('Enter the distance between Cross-sections')
    disp(i)
    disp('and')
    disp(i+1)
    dist = input('');   %prompts user for distance between cross-sections.
end

gap = gap + dist;

% Opens shunt file and reads data into an array
fname = ['Shunt_' int2str(i+1)];
fid = fopen(fname,'r');
Skip_shunt = fscanf ( fid,'%s', [1,2]); % Gets rid of X Y header in file
Shunt_data = fscanf ( fid,'%i'); % Reads data into an N x 1 array
fclose(fid);
SectionX = Shunt_data(1:2:length(Shunt_data));  % Puts X data into an Nx1 array
SectionY = Shunt_data(2:2:length(Shunt_data));  % Puts Y data into an Nx1 array

SectionX = SectionX/49.5;   %   Converts pixels to mm (0.014085 mm/pixel).Number found
SectionY = SectionY/49.5;   %   in Quantum using calibration file

meanX = mean (SectionX);
meanY = mean (SectionY);

for j=1:length(SectionX)/interval
    xcoor(j)=SectionX(interval*j-interval+1)/1;
    ycoor(j)=SectionY(interval*j-interval+1)/1;
    zcoor(j)=gap;

   %  Method 1:  Setting up guidelines for the loft to follow (4 lines)
   %  Takes the min & max points along both axes and uses those points
   %  from each section to make a guideline
   if xcoor(j)>xmax
        xmax=xcoor(j);
```

```
        ypt_xmax=ycoor(j);
    end

    if ycoor(j)>ymax
        ymax=ycoor(j);
        xpt_ymax=xcoor(j);
    end

    if ycoor(j)<xmin
        ymin=ycoor(j);
        xpt_ymin=xcoor(j);
    end

    if xcoor(j)<xmin
        xmin=xcoor(j);
        ypt_xmin=ycoor(j);
    end

   zpt_xmin=zcoor(j);
   zpt_xmax=zcoor(j);
   %  End of setting up guidelines for Method 1

   %  Method 2:  Setting up guidelines based upon the centroid of each section
   %  Minimum Y pt:
   if xcoor(j)<(1.2*meanX) & xcoor(j)>(.8*meanX) & ycoor(j)<meanY &
       (abs(xcoor(j)-meanX))<(abs(baseX-meanX))
     baseY = ycoor(j);
     baseX = xcoor(j);
     baseZ = zcoor(j);
   end
   %  end of Method 2

end

% To close section (make a closed loop so that last data point is
% equivalent to first data point in loop)
v=length(SectionX)/interval +1;
v=int8(v);
xcoor(v)=SectionX(1)/1;
ycoor(v)=SectionY(1)/1;
zcoor(v)=gap;

X=[xcoor' ycoor' zcoor'];
fname2 =['c:\Tim\Shunt\Quantim_Files\Shunt4.0@3.5\cross_section_4_' int2str(i+1) '.txt'];
fid = fopen(fname2,'w');
fprintf(fid,'%4.4f\t %4.4f\t %4.4f\n',(X')); %write output file
fclose(fid);

% Writes four points from each section that are the maximum and minimum x and y values;
% needed to generate a curve through each cross-section

Path1=[xpt_ymin ymin zpt_xmax];
```

```
    fname5 =['c:\Tim\Shunt\Quantim_Files\Shunt4.0@3.5\pathway1_4_' int2str(numb) '.txt'];
    fid = fopen(fname5,'a');
    fprintf(fid,'%4.4f\t %4.4f\t %4.4f\n',Path1);
    fclose(fid);

    Path2=[baseX baseY baseZ];
    fname6 =['c:\Tim\Shunt\Quantim_Files\Shunt4.0@3.5\realpath_4_' int2str(numb) '.txt'];
    fid = fopen(fname6,'a');
    fprintf(fid,'%4.4f\t %4.4f\t %4.4f\n',Path2);
    fclose(fid);

    Path3=[xmax ypt_xmax zpt_xmax];
    fname5 =['c:\Tim\Shunt\Quantim_Files\Shunt4.0@3.5\pathway3_4_' int2str(numb) '.txt'];
    fid = fopen(fname5,'a');
    fprintf(fid,'%4.4f\t %4.4f\t %4.4f\n',Path3);
    fclose(fid);

    Path4=[xmin ypt_xmin zpt_xmin];
    fname6 =['c:\Tim\Shunt\Quantim_Files\Shunt4.0@3.5\pathway4_4_' int2str(numb) '.txt'];
    fid = fopen(fname6,'a');
    fprintf(fid,'%4.4f\t %4.4f\t %4.4f\n',Path4);
    fclose(fid);


end
```

C.1.2 Mask Generation

```
%FIRST MASK
function maskmodi(position)

% % run=int2str(run);
% position=int2str(position);

path1='c:\xcap\shunt\Arterial_Tree\07.14.03\';

%normal
% maskfile=strcat(path1,'mask',run,'_10bit.bin')
% maskfile2=strcat(path1,'mask',run,'_8bit.bin')

% %for latest shunt runs
maskfile=strcat(path1,'mask10s_1_10bit.bin')
maskfile2=strcat(path1,'mask10s_1_8bit.bin')

nxc=1008;
nyc=1018;
colormap(gray);

% load 10 bit xcap image as 16 bit image
fid=fopen(maskfile,'r');
maskimage=fread(fid,[nxc,nyc],'int16');
```

```
st=fclose(fid);

figure(1);
imagesc(maskimage.'),axis off,axis equal,title('original 10 bit mask');

junk=maskimage;
% set values in array to floor and ceiling of the raw xcap image
for i=1:nxc;
    for j=1:nyc;
        if maskimage(i,j)>200;
            maskimage(i,j)=255;
        else
            maskimage(i,j)=0;
        end
    end
end

%save the mask file(s)
fid=fopen(maskfile2,'w');
fwrite(fid,maskimage,'int8');
st=fclose(fid);

% display mask
figure(2);
colormap(gray);
imagesc(maskimage.'),axis off,axis equal,title('final 8 bit mask');
end
```

C.1.3 Post-processing

```
function shuntpiv

%set base path of files
basepath='c:\piv\processed\shunt\04.14.03\';  %must add Trial2\ for position 2 of 5mm shunt

%run number
    tube=7
%steady (s)or pulsatile (p)?
    type='p'
%trial number
    trial=1    %must be trial=2 for position 2 of tube 8 (5mm shunt ran on 04.22.03)
%position
    position=4
%number of tensor files
    % 128 - for runs 7p and 8p
    % 31  - for runs 5s and 5p, position 2 only
    % 112 - for run 9p trial 3 only
    % 62  - for all other runs
    ntot=128

savefile=strcat('tube',int2str(tube),type,int2str(trial),int2str(position),'.mat')
```

```
%conversion info - spatial and temporal scales to give units in cm/s
scale=741  %pixels/cm 741 for 4mm & 5mm shunt (tube 7,8), 613 for 3.5mm shunt (Tube 9)

pulse=160;  %160 for 3.5, 4 & 5 mm shunts ran on 05.19.03, 04.14.03 and 04.22.03

speed=0;

%Parameters for skin friction plots
%Tube 7: 1 pulse cycle~ (1)10-31 (2)85-105 (3)24-47 (4)37-57
%Tube 8: 1 pulse cycle~ (1)3-16  (2)11-24  (3)37-50 (4)69-82
    nstart_cf=1;    %image to start with
    ntot_cf=2;    %Number of images to include, ~33 for one pulse cycle of tubes 7,8
    factor_cf=3;    %plot every x image
    uf=25            %uf (characteristic velocity) determined by mean(mean(u)) in cm/s
    uf_start=21;    %starting and ending rows to look at for calculating uf and umean
    uf_end=49;      %(don't need zeros)
    mu=0.00009438;   %N*s/cm^2
    p=.0009982;     %p = kg/cm^3
    row_cf=47;      %row to be looked at.  Run grid_values to see what row is near wall,
                    %see below:(top,bottom)
                    %Tube 7: pos1:(? & 50) pos2:(? & 50) pos3:(21 & 49) pos4:(19 & 48)
                    %Tube 8: pos1:(21 & ?) pos2:(21 & ?) pos3:(22 & ?) pos4:(21 & 50)
                    %Tube 9: pos1:(17 & 41)
    row_sh=17;
    col_sh=31;      %row and coloumn for finding shear stress at specific point over time
    export_shear_data=1;         %1 for yes, 2 for no.  To export files for shear rate
                                 %comparison and mean cf
    export_laminar_data=2;    %1 for yes, 2 for no.  To export files for determing
                              %turbulent or laminar flow comparison between tubes

%Parameters for calculating shear stress
%viscoblood=1.06*.030
viscoblood=.032
%conversion factors to cm/s
convel=(scale*pulse/1000000);
convor=(pulse/1000000);

%check array size
k=1; [ny,nx]=tensfunc2(tube,type,trial,position,k,basepath)

%create empty arrays
uav=zeros(ntot,nx,ny);
vav=zeros(ntot,nx,ny);
vortav=zeros(ntot,nx,ny);
contav=zeros(ntot,nx,ny);
un=zeros(nx,ny);
vn=zeros(nx,ny);
vorn=zeros(nx,ny);
conn=zeros(nx,ny);
corn=zeros(nx,ny);
ctr=zeros(nx,ny);
```

```
urms=zeros(nx,ny);
dvdxn=zeros(nx,ny);
dudyn=zeros(nx,ny);
wall_cf=zeros(ntot,ny);

%initializing variables for determining maximum values
point_max_dudy=0;
point_max_u=0;
point_max_vort=0;
image_number=0;
shear_stress_point=0;
dudy_any_point=0;
velocity_point=0;
sampling_rate=0;
mean_dudy_wall=0;

%read in data files
for i=1:ntot
    % i=38;
    [u,v,vort,cont,corr,dvdx,dudy]=tensfunc(tube,type,trial,position,i,basepath);
                                    %miner(run number, data set, frame, base path)
    un=u+un;
    vn=v+vn;

    vorn=vort+vorn;
    conn=cont+conn;
    corn=corr+corn;
    uav(i,:,:)=u;
    vav(i,:,:)=v;
    vortav(i,:,:)=vort;
    contav(i,:,:)=cont;
    dvdxn=dvdxn+dvdx;
    dudyn=dudyn+dudy;
    for j=1:nx
        for k=1:ny
            if u(j,k) < 0
                ctr(j,k)=ctr(j,k)+1;
            end
        end
    end

    %Determing max values
    if (max(max(abs(dudy)))>point_max_dudy)
        point_max_dudy=max(max(abs(dudy)));
        image_number=i;
    end
    if max(max(abs(vort)))>point_max_vort
        point_max_vort=max(max(abs(vort)));
    end
    if max(max(abs(u)))>point_max_u;
        point_max_u=max(max(abs(u)));
    end
```

```
    %Determining skin friction across wall for each image
    shear_point=zeros(nx,ny);
    cf=zeros(nx,ny);
    shear_point = mu.*dudy;
    cf=shear_point./(0.5*.0009982*uf^2); %did not yet divide by uf^2(char. vel)
    wall_cf(i,:)=cf(row_cf,:);

    %Determining shear stress at specific point
    shear_stress_point(i)=dudy(row_sh,col_sh);
    %Determing velocity at specific point
    velocity_point(i)=u(row_sh,col_sh);

    ctr=-ctr;
    offset=0;
    xllim=3;
    yllim=5;
    xulim=nx-offset;
    yulim=ny-(offset);
    yllim=15;
    yulim=55;

end


%%%%%%%%%%%%%% PROCESSING %%%%%%%%%%%%%%%%%%%%

%caclulate averages
un=un/ntot;
vn=vn/ntot;
vorn=vorn/ntot;
conn=conn/ntot;
corn=corn/ntot;
dvdxn=dvdxn/ntot;
dudyn=dudyn/ntot;
ctr=-ctr/ntot;

%scale data
un=un/convel;
vn=vn/convel;
vorn=vorn/convor;
dudyn=dudyn/convor;
point_max_dudy=point_max_dudy/convor;
point_max_vort=point_max_vort/convor;
point_max_u=point_max_u/convel;
wall_cf=wall_cf/convor;
shear_stress_point=shear_stress_point/convor;
velocity_point=velocity_point/convel;


fprintf('\nThinking....')
```

```
%calculate rms turbulence
for j=1:nx
    fprintf('.')
        for k=1:ny
            dum1=0; dum2=0; dum3=0;
            for i=1:ntot
                dum1=sqrt(un(j,k)^2+vn(j,k)^2);
                dum2=sqrt(uav(i,j,k)^2+vav(i,j,k)^2);
                dum3=(dum1-dum2)^2+dum3;
            end
            urms(j,k)=(sqrt(dum3)/ntot);
        end
    end


%size(cf)

%calculate average maximum quantities
mag=sqrt(un.^2+vn.^2);
maxu=max(max(abs(un)));
maxmag=max(max(mag));
maxvor=max(max(abs(vorn)));
maxrms=max(max(urms));
maxdudyn=max(max(abs(dudyn)));

%calculating shear stresses
% wall_cf=wall_cf/(uf^2);       %need to divide by char. velocity (mean(mean(u)))
point_max_shear=viscoblood*point_max_dudy;
average_max_shear=viscoblood*maxdudyn;
dudy_any_point=shear_stress_point;  %dudy at any specified pt. (row,col in begin.)

%calculating average skin friction at wall over all cycles
shear=zeros(nx,ny);
cf=zeros(nx,ny);
shear=mu.*dudyn;
cf=shear./(0.5*.0009982*uf^2); %p = kg/cm^3
mean_cf=cf(row_cf,:);
mean_dudy_wall=dudyn(row_cf,:);

fprintf('\n\n Average Maximum streamwise velocity ',maxu,std(max(abs(un))));
fprintf(' Average Maximum velocity magnitude ',maxmag,std(max(abs(mag))));
fprintf(' Average Maximum vorticity ',maxvor,std(max(abs(vorn))));
fprintf(' Average Velocity fluctuation is ',maxrms/maxu*100,std(max(abs(urms))));

fprintf(' Maximum velocity during systole ',point_max_u,std(max(abs(un))));
fprintf(' Maximum vorticity during systole ',point_max_vort,std(max(abs(vorn))));

fprintf('\n Average Maximum Shear rate ',maxdudyn,std(max(abs(dudyn))));
fprintf(' Average Maximum Shear Stress ',average_max_shear);

fprintf('\n Maximum Shear rate at systole ',point_max_dudy,std(max(abs(dudyn))));
fprintf(' Maximum Shear Stress in blood ',point_max_shear);
```

```
fprintf(' and occurs in image %8.1f',image_number);

save(savefile,'un','vn','vorn','ctr','dvdxn','dudyn','cf');

offset=0;
xllim=3;
yllim=5;
xulim=nx-offset;
yulim=ny-(offset);
yllim=15;
yulim=55;

%set edge regions to zero if need be
un(:,1)=0; vn(:,1)=0; vorn(:,1)=0;
un(:,2)=0; vn(:,2)=0; vorn(:,2)=0;
%un(1,:)=0; vn(1,:)=0; vorn(1,:)=0;
un(:,ny-1)=0; vn(:,ny-1)=0; vorn(:,ny-1)=0;
un(:,ny)=0; vn(:,ny)=0; vorn(:,ny)=0;

%new colormap
jet2=abs(jet-1);

%vertices for patch command for slab (if needed)
xc=9; yc=27;
x=[1 81 81 xc xc 1];
y=[45 45 40 40 yc yc];

%end of main routine
% PLOTS

%skin friction plot (mean cf and cf over time)
walldist=linspace(0,1,ny);
if position==1
    walldist_temp=walldist;
    for i=0:1:(ny-1)
        walldist(ny-i)=walldist_temp(i+1);
    end
    walldist=walldist*2;
end
if position==3
    walldist=walldist*2;
end
if position==4
    walldist=walldist*2+2;
end

flipping figures; need - for tube 7
wall_cf=-wall_cf;
shear_stress_point=-shear_stress_point;
```

```
figure(9);      %3D graph of cf along wall of tube over pulse cycle
width_cf=ntot_cf-nstart_cf;
factor_cf=1;
temp_wall_cf=zeros(width_cf,62);
count=1;
for i=nstart_cf:factor_cf:ntot_cf
    temp_wall_cf(count,:)=wall_cf(i,:);
    count=count+factor_cf;
end
surf_xaxis=0:width_cf;
size(surf_xaxis)
size(walldist)
size(temp_wall_cf)
count=count-factor_cf;
temp_wall_cf(count,:)=0;  %make last row zero so graph looks better
surf(walldist,surf_xaxis,temp_wall_cf);

ylabel('Phase of pulse cycle');
xlabel('Distance downstream from throat');
zlabel('Skin Friction Coefficient at wall');


figure(10); %plot of shear stress at specific point in tube over one cycle
plot(shear_stress_point(1:128))
ylabel('Shear rate  (s\it^{-1})');
xlabel('Phase of pulse cycle');

if export_shear_data==1
    %exporting dudy_any_point to file for comparison among positions
    file_name=strcat('c:\dudy_pos_',int2str(tube),'_',int2str(position),'.txt');
    fid=fopen(file_name,'w');
    fprintf(fid,'%f\n',dudy_any_point(nstart_cf:ntot_cf));
    fclose(fid);
    %exporting mean(wall_cf) to file for comparison among other tubes
    file_name=strcat('c:\wall_cf_',int2str(tube),'_',int2str(position),'.txt');
    fid=fopen(file_name,'w');
    fprintf(fid,'%f\n',mean(wall_cf));
    fclose(fid);
    %exporting mean_dudy_wall to file for comparison among other tubes
    file_name=strcat('c:\mean_dudy_wall_',int2str(tube),'_',int2str(position),'.txt');
    fid=fopen(file_name,'w');
    fprintf(fid,'%f\n',mean_dudy_wall);
    fclose(fid);
    plot(mean_dudy_wall);
end

if export_laminar_data==1
    %exporting umean to file for comparison among positions
    file_name=strcat('c:\umean_pos_',int2str(tube),'_',int2str(position),'.txt');
    fid=fopen(file_name,'w');
    fprintf(fid,'%f\n',umean);
    fclose(fid);
```

```
    %exporting re to file for comparison among other tubes
    file_name=strcat('c:\re_pos_',int2str(tube),'_',int2str(position),'.txt');
    fid=fopen(file_name,'w');
    fprintf(fid,'%f\n',re);
    fclose(fid);
    plot(re);
end

return

pause


ninput=4;
[tx,ty]=ginput(ninput)

figure(16)
for i=1:ninput
    ix=round(tx(i))
    iy=round(ty(i))
    plot(uav(:,ix,iy),'ro--');
    hold on
end

hold off
%
%end of main routine
return;


%%%%%%%%%%%%%%%%%%%%%%%%%%%%%%%%%%%%%%%%%%%%%%%%%%%%%%%%%%%%%%%%%%%%%%%%%%%%%%%
%%%%%%%%%%%%%%%%%%%%%%%%%%%%%%%%%%%%%%%%%%%%%%%%%%%%%%%%%%%%%%%%%%%%%%%%%%%%%%%

function [e1,e2,vorticity,continuity,corr,dvdx,dudy]=
tensfunc(tube,type,trial,position,batch,basepath)

tube=int2str(tube);
trial=int2str(trial);
position=int2str(position);
bat=int2str(batch);

% file and path names

if batch < 10
    bat=strcat('.00',bat);
else
    if batch < 100
        bat=strcat('.0',bat);
    else
        bat=strcat('.',bat);
    end
end
```

```
lptfile=strcat('run_',tube,type,trial,'_',position,bat);
lptima1=strcat('image1.lpt');lptima2=strcat('image2.lpt');


u_infinity=0;
v_infinity=0;



%SET PATHS AND FILE NAMES
path=strcat(basepath);
%path=strcat('c:\piv\xcap\mine\images\run',run,'\');
rdfile=strcat(path,lptfile);
imfile1=strcat(path,lptima1);
imfile2=strcat(path,lptima2);

% read data file into header and tensor arrays

fprintf(' Reading single tensor file %s in %s\n',lptfile,path)

fid=fopen(rdfile,'r','ieee-le');
header=fread(fid,64,'int16');
  version=header(1);                % walpt version number
  nxc =header( 2) ; nyc =header( 3); % camera size
  nxuv=header( 4) ; nyuv=header( 5); % velocity array size
  nxw =header( 6) ; nyw =header( 7); % window sizes in pixels
  nxs =header( 8) ; nys =header( 9); % step sizes in pixels
  nxf =header(10) ; nyf =header(11); % flow region size in pixels
  xf  =header(12) ; yf  =header(13); % flow region offset in pixels
  nbits=header(14);                 % pixel depth of original flow images
  % utensor=[nxuv,nyuv,7]
  % read tensor components from file in succession
  e1=fread(fid,[nxuv,nyuv],'float'); % u
  e2=fread(fid,[nxuv,nyuv],'float'); % v
  e3=fread(fid,[nxuv,nyuv],'float'); % du/dx
  e4=fread(fid,[nxuv,nyuv],'float'); % dv/dx
  e5=fread(fid,[nxuv,nyuv],'float'); % du/dy
  e6=fread(fid,[nxuv,nyuv],'float'); % dv/dy
  e7=fread(fid,[nxuv,nyuv],'float'); % correlation
st=fclose(fid);

%rotate fields
e1=e1.';
e2=e2.';
e3=e3.';
e4=e4.';
e5=e5.';
e6=e6.';
e7=e7.';

% add (subtract) v_infinity to the velocity field to change
```

```
% reference frames to object's frame for tow-tank
% runs.  Set u_infinity to zero to run in lab frame.

for i=1:nyuv
   for j=1:nxuv
      if e1(i,j)<=999
         e1(i,j)=e1(i,j)-u_infinity;
      end
   end
end

for i=1:nyuv
   for j=1:nxuv
      if e2(i,j)<=999
         e2(i,j)=e2(i,j)+v_infinity;
      end
   end
end

% Check and replace the "missing" 1000 in velocity
% fields with zeros (option XXXX in walpt).
% (This option is for use with IDL or similar programs.)

for i=1:nyuv
   for j=1:nxuv
   if e1(i,j) > 999
         e1(i,j) = 0;
         end
         if e2(i,j) > 999
            e2(i,j) = 0;
         end
    end
end

%Items to return
corr=e7;

% Calculate vorticity,continuity

vorticity=e5-e4;    %du/dy-dv/dx
continuity=e3+e6;   %du/dx+dv/dy

%return velocity gradient for wall skin friction calculation
%(in this case, dv/dx)

dvdx=e4;
dudy=e5;

return

function [nx,ny]=tensfunc2(tube,type,trial,position,batch,basepath)
```

```
tube=int2str(tube);
trial=int2str(trial);
position=int2str(position);
bat=int2str(batch);

% file and path names

if batch < 10
    bat=strcat('.00',bat);
else
    if batch < 100
        bat=strcat('.0',bat);
    else
        bat=strcat('.',bat);
    end
end

lptfile=strcat('run_',tube,type,trial,'_',position,bat);
lptima1=strcat('image1.lpt');lptima2=strcat('image2.lpt');

u_infinity=0;
v_infinity=0;

%SET PATHS AND FILE NAMES
path=strcat(basepath);
%path=strcat('c:\piv\xcap\mine\images\run',run,'\');
rdfile=strcat(path,lptfile);
imfile1=strcat(path,lptima1);
imfile2=strcat(path,lptima2);

% read data file into header and tensor arrays

fprintf(' Reading tensor file %s in %s to determine array size\n',lptfile,path)

% fid=fopen(rdfile,'r','ieee-le');
fid=fopen(rdfile,'r');
[FILENAME,PERMISSION,MACHINEFORMAT] = fopen(fid)
header=fread(fid,64,'int16');
  version=header(1);                % walpt version number (starting with 300)
  nxc =header( 2);  nyc =header( 3); % camera size
  nxuv=header( 4) ; nyuv=header( 5); % velocity array size
  nxw =header( 6) ; nyw =header( 7); % window sizes in pixels
  nxs =header( 8) ; nys =header( 9); % step sizes in pixels
  nxf =header(10) ; nyf =header(11); % flow region size in pixels
  xf  =header(12) ; yf  =header(13); % flow region offset in pixels
  nbits=header(14);                 % pixel depth of original flow images
  % utensor=[nxuv,nyuv,7]
  % read tensor components from file in succession
  e1=fread(fid,[nxuv,nyuv],'single'); % u
  e2=fread(fid,[nxuv,nyuv],'float'); % v
  e3=fread(fid,[nxuv,nyuv],'float'); % du/dx
  e4=fread(fid,[nxuv,nyuv],'float'); % dv/dx
```

```
  e5=fread(fid,[nxuv,nyuv],'float'); % du/dy
  e6=fread(fid,[nxuv,nyuv],'float'); % dv/dy
  e7=fread(fid,[nxuv,nyuv],'float'); % correlation
st=fclose(fid);

nx=nxuv;
ny=nyuv;

return
```

C.2 Sample WaLPT Input File

```
lptmode, 0=singlepass, 1=small to large, 2=large to small, 3= LPT
2 1 0 1
input file names ( one line per file )
run_8p1_4.lst
run_8p1_4
image size nxc, nyc, pixr
1008 1018 10 1.00
flow size, nxf, nyf
1008 1018
flow offset, xf, yf
0 0
window size, nxw, nyw, 2**n
32 32
amod, min, max windows dimensions 2**n, correlaltion level corlvl
1 8  32 0.50
step size, nxs, nys
16 16
window type, wtype 1-7, see source listing
1
peak type, ptype 0=grid,1=parabolic,2=gaussian
2
laundary type, ltype 0=no laundering,1=rejection
0
extension parameter, 0= none, zero padding, 1= smooth (nth order)
0
filter widths (1/) fltrwx,fltrwy; 0= no filtering, 1,2,.. higher ; nfil
10 10 3
wall parameters: nwalls, parex, motion, intflag, outmask
2 1 0 0 1
wall geometry file
c:\xcap\shunt\04.22.03\mask8_4_8bit.bin
motion parameters: dxcg, dycg ,rot
0.00 0.00 0.00
0.00 0.00 0.00
0.00 0.00 0.00
```

Bibliography

[1] Amato, J.J., Marbey, M.L., Bush, C., Galdieri, R.J., Cotroneo, J.V., and Bushong, J. "Systemic-Pulmonary Polytetrafluoroethylene Shunts in Palliative Operations for Congenital Heart Disease. Revival of the Central Shunt," *Journal of Thorasic Cardiovascular Surgery*, Vol. 95, 1988, pp. 62-69.

[2] Hennein, H.A., and Bove, E.L. *Hypoplastic Left Heart Syndrome*. Futura Publishing Company, Armonk, 2002.

[3] Stroud, J.S., Berger, S.A., and Saloner, D. "Influence of Stenosis Morphology on Flow Through Severely Stenotic Vessels: Implications for Plaque Rupture," *Journal of Biomechanics*, Vo. 33, No. 4, 2000, pp. 443-455.

[4] Zhang, J., Bergeron, A.L., Yu, Q., Sun, C., McIntire, L.V., Lopez, J.A., and Dong, J. "Platelet Aggregation and Activation Under Complex Patterns of Shear Stress," *Journal of Thrombosis and Haemostasis*, Vol. 88, 2002, pp. 817-821.

[5] Norwood, W.I., Lang, P., Casteneda, A.R., and Campbell, D.N. "Experience with Operations for Hypoplastic Left Heart Syndrome," *Journal of Thorasic Cardiovascular Surgery*, Vol. 82, No. 4, 1981, pp. 511-519.

[6] Daebritz, S.H., Nollert, G.D., Zurakowski, D., Khalil, P.N., Lang, P., del Nido P.J. et al. "Results of Norwood Stage I Operations; Comparison of Hypoplastic Left Heart Syndrome with other Malformations," *Journal of Thorasic Cardiovascular Surgery*, Vol. 119, 2000, pp. 358-367.

[7] Gutgesell, H.P., and Gibson, J. "Management of Hypoplastic Left Heart Syndrome in the 1990s," *American Journal of Cardiology*, Vol. 89, No. 7, 2002, pp. 842-846.

[8] Mahle, W.T., Spray, T.L., Wernovsky, G., Gaynor, J.W., and Clark III, B.J. "Survival After

Reconstructive Surgery for Hypoplastic Left Heart Syndrome: a 15-year Experience from a Single Institution," *Circulation*, Vol. 102, 2000, pp. III136-III141.

[9] Bartram, U., Grunenfelder, J., and Van Praagh, R. "Causes of Death After the Modified Norwood Procedure: a Study of 122 Postmortem Cases," *Annuals of Thorasic Surgery*, Vol. 64, 1997, pp. 1795-1802.

[10] Jobes, D.R., Nicolson, S.C., Steven, J.M., Miller, M., Jacobs, M.L., and Norwood, W.I. "Carbon Dioxide Prevents Pulmonary Overcirculation in Hypoplastic Left Heart Syndrome," *Annuals of Thorasic Surgery*, Vol. 54, 1992, pp. 150-151.

[11] Schmid, F.X., Kampmann, C., Wlodimierz, K., Choi, Y., Knuf, M., Tzanova, I., and Oelert, H. "Adjustable Tourniquet to Manipulate Pulmonary Blood Flow After Norwood Operations," *The Society of Thoracic Surgeons*, Vol. 68, 1999, pp. 2306-2309.

[12] Chikada, M., Sekiguchi, A., Oho, S., Miyamoto, T., Ishida, R., Takayama, H., and Ishizawa, A. "Dilatable Banding of a Blalock-Taussig Shunt," *The Society of Thoracic Surgeons*, Vol. 74, 2002, pp. 253-255.

[13] Kuduvalli, M., McLaughlin, K.E., Trivedi, D.B., and Pozzi, M. "Norwood-Type Operation with Adjustable Systemic-Pulmonary Shunt using Hemostatic Clip," *Annuals of Thoracic Surgery*, Vol. 72, No. 2, August 2001, pp.634-635.

[14] Song, M., Sato, M., and Ueda, Y. "Three-Dimensional Simulation of the Blalock-Taussig Shunt Using Computational Fluid Dynamics, *Surgery Today*, Vol. 31, March 2001, pp. 688-694.

[15] Migliavacca, F. et al. "Modeling of the Norwood Circulation: Effects of Shunt Size, Vascular Resistances, and Heart Rate, *American Journal of Physiology: Heart and Circulatory Physiology*, Vol. 280, No. 5, May 2001, pp. 2076-2086.

[16] Cincinnati Children's Hospital Medical Center. http://www.cincinnatichildrens.org/, August 2002.

[17] Zamir, M. *The Physics of Pulsatile Flow*, Springer-Verlag, New York, 2000.

[18] Evett, J.B., and Liu, C. *Fundamentals of Fluid Mechanics*, McGraw-Hill, New York, 1987.

[19] Shirazi, M. "Theory of Arterial Circulation." *University of Dayton Research Institute*, Wright-Patterson Air Force Base, February 1972.

[20] Smith, L.N., and Schimmel, K. "Blood Rheology at Eleveated Hematocrits," *Ron McNair Symposium on Science Frontiers*, January, 2002.

[21] Lim, W.L., Chew, .T., Chew, T.C.,and Low, H.T. "Pulsatile Flow Studies of a Porcine Bioprosthetic Aortic Valve in vitro: PIV Measurements and Shear-Induced Blood Damage," *Journal of Biomechanics*, Vol.34, July 2001, pp. 1417-1427.

[22] Wurzinger, L.J., Opitz, R., Blasberg, P., and Schmid-Schonbein, H. "Platelet and Coagulation Parameters Following Millisecond Exposure to Laminar Shear Stress, *Journal of Thrombosis and Haemostasis*, Vol. 54, No. 2, August 1985, pp. 381-386.

[23] Lu, P.C., Lai, H.C., and Liu, J.S. "A Reevaluation and Discussion on the Threshold Limit for Hemolysis in a Turbulent Shear Flow," *Journal of Biomechanics*, Vol. 34, No. 10, 2001, pp. 1361-1364.

[24] Iwamoto, S., *et al.* . "The Release Mechanism of Platelet-Activating Factor during Shear-Stress Induced Platelet Aggregation," *Biochemical and Biophysical Research Communications*, No. RC977435, 1997, pp. 101-105.

[25] Schmugge, M., Rand, M.L., and Freedman, J. "Platelets and von Willebrand Factor," *Transfusion and Apheresis Science*, Vol. 28, No. 3, June 2003, pp. 269-277.

[26] Anderson, G.H., Hellums, J.D., Moake, J.L, and Alfrey, C.P. Jr. "Platelet Lysis and Aggregation in Shear Fields," *Blood Cells*, Vol. 4, No. 3, 1978, pp. 499-511.

[27] Pennati, G., Fiore, G.B., Migliavacca, F., Lagana, K., Fumero, R., and Dubini, G. "In Vitro Steady-Flow Analysis of Systemic-to-Pulmonary Shunt Haemodynamics," *Journal of Biomechanics*, Vol. 34, No. 1, January 2002, pp. 23-30.

[28] Ratner, B.D., Hoffman, A.S., Schoen, F.J., and Lemons, J.E. *Biomaterials Science: An Introduction to Materials in Medicine,* Academic Press, San Diego, 1996.

[29] Douglas, W. M.D. Personal Communications.

[30] Migliavacca, F., Yates, R., Giancarlo, P., Gabriele, D., Roberto, F., and de Leval, M.R. "Calculating blood flow from Doppler measurements in the systemic-to-pulmonary artery shunt after the Norwood operation: a method based on computational fluid dynamics," *Ultrasound in Medicine and Biology*, Vol.26, No. 2, 2000, pp. 209-219.

[31] Raffel M., Willet, C., and Kompenhans, J. *Particle Image Velocimetry: A Practical Guide*, Springer-Verlag Press, Berlin, 1998.

[32] Jacob, J., Douglas, W., and Knapp, C. "Constriction Effects in an In Vitro Model of an Adjustable Systemic-Pulmonary Artery Shunt," *Bulletin of the American Physical Society*, Vol. 46, No. 10, 2001, pp. 100-101.

[33] Zarandi, M., Dabiri, D., and Gharib, M. "Application of Digital Ultrasound Speckle Image Velocimetry (DUSIV) for Quantitative Flow Measurements in Aortic Vessel: an In Vitro Study," *Bulletin of the American Physical Society*, Vol. 46, No. 10, 2001, pp. 99.

[34] Roclawski, H. "PIV Measurements of Channel Flow with Multiple Rib Arrangements." M.S. Thesis, University of Kentucky, 2001.

[35] M. J. Sholl and Ö Savaş. "A fast Lagrangian PIV Method for Study of General High-Gradient Flows." *AIAA 35th Aerospace Meetings & Exhibits.* AIAA, 1997. Paper 97-0493.

Vita

Timothy Marc Brown was born in Harare, Zimbabwe in 1978. Son of missionary parents, he grew up along the coast in South Africa before coming to America in 1992. He went to Western Kentucky University in 1996 where he played on the varsity tennis team. Two years later he transferred to the University of Kentucky, where he received his B.S. in Mechanical Engineering in 2001. As an undergraduate, Timothy was an officer in Phi Tau Sigma, an honorary mechanical engineering society, member of the Freshman Leadership Council for the BSU, and on the Engineering Student Council. He was also nominated to the Golden Key Award Society and the National Dean's List ('96-'02). In 2002, he began working on his Master's Degree in Biomedical Engineering. As a graduate student, he presented his research at several conferences and was the second runner-up in the graduate division at the 2003 AIAA regional conference for presentation of his research.